Analysis of *Epichloë festucae* small secreted proteins in the interaction with *Lolium perenne*

Berit Hassing[1,2], David Winter[1,2], Yvonne Becker[3], Carl H. Mesarich[1,4], Carla J. Eaton[1,2], Barry Scott[1,2]

[1]Institute of Fundamental Sciences, Massey University, Palmerston North, New Zealand

[2]Bio-Protection Research Centre, New Zealand

[3] Institute for Epidemiology and Pathogen Diagnostics, Julius Küehn-Institute, Federal Research Centre for Cultivated Plants, Braunschweig, Germany

[4]School of Agriculture and Environment, Massey University, Palmerston North, New Zealand

* Corresponding author

E-mail: d.b.scott@massey.ac.nz (BS)

Abstract

Epichloë festucae is an endophyte of the agriculturally important perennial ryegrass. This species systemically colonises the aerial tissues of this host where its growth is tightly regulated thereby maintaining a mutualistic symbiotic interaction. Recent studies have suggested that small secreted proteins, termed effectors, play a vital role in the suppression of host defence responses. To date only a few effectors with important roles in mutualistic interactions have been described. Here we make use of the fully assembled *E. festucae* genome and EffectorP to generate a suite of 141 effector candidates. These were analysed with respect to their genome location and expression profiles *in planta* and in several symbiosis-defective mutants. We found an association between effector candidates and a class of transposable elements known as MITEs, but no correlation with other dynamic features of the *E. festucae* genome, such as transposable element-rich regions. Three effector candidates and a small GPI-anchored protein were chosen for functional analysis based on their high expression *in planta* compared to in culture and their differential regulation in symbiosis defective *E. festucae* mutants. All three candidate effector proteins were shown to possess a functional signal peptide and two could be detected in the extracellular medium by western blotting. Localization of the effector candidates *in planta* suggests that they are not translocated into the plant cell, but rather, are localized in the apoplastic space or are attached to the cell wall. Deletion and overexpression of the effector candidates, as well as the putative GPI-anchored protein, did not affect the plant growth phenotype or restrict growth of *E. festucae* mutants *in planta*. These results indicate that these

proteins are either not required for the interaction at the observed life stages or that there is redundancy between effectors expressed by *E. festucae*.

Introduction

Plant-pathogenic fungi deploy a number of virulence factors, termed effector proteins, to promote colonization of their hosts. These effector proteins, which can be targeted to the host apoplast (extracellular effectors) or to various compartments of the plant cell (intracellular effectors), typically promote colonization by altering host physiology or by modulating host immune responses [1]. Well-characterized examples of extracellular fungal effector proteins include Avr2, Avr4 and Ecp6 from the tomato leaf mould pathogen *Cladosporium fulvum* [2-4], as well as Pit2 and Rsp3 from the corn smut pathogen *Ustilago maydis* [5, 6]. More specifically, Avr4 binds to chitin molecules present in the cell wall of invading hyphae to prevent hydrolysis by host chitinases [2, 7], while Ecp6 sequesters chitin oligosaccharides released from the cell wall of invading hyphae to prevent detection by host chitin immune receptors [4, 8]. Rsp3 binds to the cell wall of invading hyphae to protect them against two antimicrobial mannose-binding host proteins [6], while both Pit2 and Avr2 inhibit host cysteine proteases to prevent degradation of fungal proteins [3, 9-11]. A well-characterized example of an intracellular fungal effector protein is Cmu1 from *U. maydis*, which functions as a chorismate mutase to redirect the metabolism of chorismate away from the production of the defense signaling hormone salicylic acid [12].

Like plant-pathogenic fungi, plant-beneficial fungi must also deploy effector proteins to promote host colonization [13, 14]. However, to date only a small number of effectors from this group of fungi have been identified and functionally characterized. Furthermore, of those that have been functionally characterized all are from mycorrhizal fungi. One such example is MiSSP7 from *Laccaria bicolor*, an ectomycorrhizal fungus of poplar roots. In plants (including poplar), JAZ proteins repress the expression of jasmonic acid (JA)-related defense genes, with the degradation of these proteins leading to the activation of JA-related defense genes [15]. During infection of poplar, MiSSP7 is transported into the plant nucleus where it interacts with and stabilizes the JAZ protein PtJAZ6 to prevent its degradation, and thus prevent the expression of JA defence-related genes [16, 17]. A second example is SP7, which is produced by the arbuscular mycorrhizal fungus, *Glomus intraradices*. SP7, which like PtJAZ6 is also transported into the plant nucleus, influences defense gene signaling by interacting with the pathogenicity-related transcription factor ERF12 [18]. A third example is Fgb1 has been characterized from the endophytic root-colonizing fungus, *Piriformospora indica*. Fgb1 is a β-glucan-binding lectin that modulates the fungal cell composition and prevents β-glucan-triggered immunity in plants, presumably through a similar mechanism to that shown for as Ecp6 and other LysM domain-containing effectors from plant-pathogenic fungi [19].

There is little amino acid sequence conservation between effector proteins of plant-associated fungi, and most lack obvious functional domains. Together, these features render their identification and functional characterization difficult. Some features, however, are common to many

effector proteins. For example, most have an amino (N)-terminal signal peptide for secretion, are small (<300 amino acid residues in length) and rich in an even number of cysteines, and are highly expressed during host colonization [1, 20]. Furthermore, many of these effector proteins are encoded by genes located in dynamic regions of the fungal genome (e.g. those regions rich in transposable elements; TEs), where increased mutation rates can result in the increased diversification of effector genes; a beneficial trait in the 'arms race' with the host [1, 21, 22]. One group of TEs are miniature inverted-repeat transposable elements (MITES)[23], which are small non-autonomous DNA transposable elements that have been proposed to have a role in regulating the expression of plant induced genes in phytopathogenic and mutualistic fungi [24-27].

Here we present an analysis of effector candidates from *Epichloë festucae*, an endophytic fungus of the cool-season grass, *Lolium perenne*. The interaction between *Epichloë spp.* and cool-season grasses is of agricultural importance due to the array of secondary metabolites produced by the endophyte that protect the host from various biotic stresses, such as insect and mammalian herbivory [28]. Unlike mycorrhizal fungi, which only infect the roots of their host plants, *E. festucae* and other *Epichloe* spp. exclusively colonize plant aerial tissues and are only found in association with their host. These endophytes can be vertically transmitted through host seeds [29, 30] or horizontally transmitted by ascospore transfer. The latter occurs following sexual development on host inflorescences, and results in the formation stromata that prevent the maturation of these inflorescences to cause 'choke' disease [31, 32]. While some *Epichloë* spp. have a high degree of host specificity, others, such as *E. typhina,* can infect a variety of grass species [33].

Within the host tissue, the fungal growth is highly restricted and confined to the intercellular spaces. Deletion of key signaling genes results in the loss of this restricted growth and, in doing so, the 'breakdown' of the symbiosis [34-40]. Here, we make use of the fully assembled *E. festucae* genome [26] and EffectorP [41] to identify a suite of candidate effectors in this mutualistic endophyte, and analyse their genomic location to identify potential patterns of distribution. In addition, we use multiple transcriptome datasets to generate an expression profile for these candidate effectors, with the aim of identifying effectors with a potential role in the *E. festucae-L. perenne* interaction. Based on these analyses, three candidate effectors were selected for functional characterization. As GPI-anchored proteins play an important role in plant–fungus interactions [42, 43] we also selected a GPI anchored protein with a similar expression file to the abovementioned candidate effectors for functional characterization.

Materials and Methods

Bioinformatics

A detailed record of the bioinformatic and statistical analyses performed in this study is provided in S1 File. Here we briefly describe each step of these analyses.

Classification of proteins and amino acid composition

The program SignalP v4.1 [44] was used to identify those *E. festucae* proteins of ≤200 amino acid residues in length that contain an N-terminal secretion signal, while EffectorP v 1.0 [41] was used to predict which of these proteins is

an effector. The latter uses a machine learning approach based on sequence properties common to known effectors. Taking these results together, each protein was then classified into one of three non-overlapping classes: (i) candidate effectors (proteins with ≤200 amino acid residues, a signal peptide and an EffectorP probability of >0.5), (ii) secreted proteins (proteins with a signal peptide that do not meet the other abovementioned criteria for effectors), and (iii) non-secreted proteins (all other proteins). The hypothesis that secreted proteins are more cysteine-rich than average was tested using a logistic regression. Specifically, a model with the proportion of cysteine residues as the response variable and membership of the three protein-classes described above as a predictor was fitted using R 3.0.1 [45].

Genomic landscape of candidate effectors

Bedtools v 2.26.0 [46] and the recently published *E. festucae* Fl1 genome [26], were used to calculate the distance between each protein-coding gene and its nearest AT-rich isochore, minature inverted TE (MITE) and telomere. Logistic regression was used to test whether secreted proteins and candidate effectors are more likely to appear near to a MITE (within 2 kb), an AT-rich isochore (within 5 kb) or a sub-telomeric region (within 50 kb) than other proteins. A Monte Carlo approach was used to test whether genes encoding candidate effectors fall into clusters within the Fl1 genome. Specifically, Bedtools was used to calculate the minimum distance between each effector-encoding gene and another gene of the same type (i.e. the minimum distance to another candidate effector gene). The mean distance between candidate effector genes was compared to a null distribution of this statistic. We simulated this null

distribution by calculating the same statistic for 1000 random gene-sets, each the same size as the set of candidate effectors.

Gene expression analyses

The hypothesis that genes encoding candidate effectors are differentially expressed *in planta* compared to axenic culture was tested by logistic regression, using previously published RNAseq data as input [36, 47]. A model in which the probability that genes demonstrate significant (corrected p-value < 0.01) and substantial (> 2 $\log_2$ fold) differences in expression between culture and *planta* conditions compared between candidate effectors, secreted proteins and all other proteins was fitted using R. Similarly, the hypothesis that repression of candidate effector genes is disrupted in Δ*hepA*, a mutant of the heterochromatin protein 1 (HP1) gene [48, 49], was tested using logistic regression. Finally, the *in planta* expression of candidate effector genes was compared across four separate symbiosis-deficient mutants, including Δ*noxA*, Δ*proA* and Δ*sakA* [36, 47] and Δ*hepA* (Chujo & Scott, personal communication. The Δ*hepA* transcriptome data used here is available from the Sequence Read Archive (SRA) under Bioproject PRJNA447872. A list of the individual biosample numbers is provided in S1 Table.

Strains and growth conditions

Escherichia coli strains were grown overnight in Lysogeny Broth (LB) or on LB agar supplemented with 100 µg/ml ampicillin or 50 µg/ml kanamycin at 37°C, as described by [50]. *Agrobacterium tumefaciens* strains were grown for one day in LB broth or for two days on LB agar supplemented with 50 µg/ml

kanamycin at 30°C, as previously described [51]. *Saccharomyces cerevisiae* strains were grown at 30°C on YPDA (2% peptone, 1% yeast extract 0.01% adenine hemisulfate, 2% glucose, 2% agar; adjusted to pH 5.7). For *S. cerevisiae* complementation assays cells were plated on CMD tryptophan dropout medium (0.67% yeast nitrogen base, 0.064% W/L dropout supplement, 0.00033% leucine, 2% sucrose, 0.1% glucose, 2% agar, pH 5.7). To test for secretion of the SUC2 secretion signal fusion protein, fresh colonies of *S. cerevisiae* were streaked on CMDRAA medium (0.67% yeast nitrogen base, 0.064% W/L dropout mixture, 0.00033% leucine, 0.00033% tryptophan, 2% raffinose, 2 µg/ml antimycin A, 2% agar, pH 5.8) and compared with growth on YPDA control plates [52, 53]. *E. festucae* strains were grown on 2.4% Potato-Dextrose Agar (PDA) supplemented with 150 µg/ml hygromycin B or 250 µg/ml geneticin or in 2.4% Potato-Dextrose Broth (PDB) for up to seven days [54, 55]. For microscopy analyses, strains were grown on 3% water agar overlaid with 1.5% water agar [40]. All strains used in this study can be found in S2 Table.

Plant growth and endophyte inoculation

E. festucae strains were inoculated into endophyte-free seedlings of perennial ryegrass (*L. perenne* cv Samson) using the method previously described [56]. Inoculated plants were grown in root trainers at 22°C in a controlled growth room with a photoperiod of 16 h light (approximately 100 µE/m^2/s) and 8 h dark. *N. benthamiana* and *N. tabacum* were grown at approx. 28°C in a controlled growth room with a photoperiod of 16 h light (approximately 100 µE/m^2/s) and 8 h dark for 6–7 weeks. For agroinfiltration experiments (see below), plants were transferred to a greenhouse and grown at 25°C with natural lighting.

211

DNA isolation, PCR and sequencing

213 High quality genomic DNA was extracted from freeze-dried mycelium of
214 *E. festucae* as previously described [57]. Plasmid DNA was extracted from *E.*
215 *coli* using the High Pure plasmid isolation kit (Roche). DNA resolved by agarose
216 gel electrophoresis was purified using the Wizard SV Gel and PCR Clean-Up
217 System (Promega) or the Zymoclean Gel DNA Recovery kit (Zymo Research).
218 PCR amplification of short DNA products was conducted with the OneTaq®
219 (NEB) polymerase according to the manufacturer's instructions. Each reaction
220 was set up as follows: 1× Standard OneTaq Reaction Buffer, 200 µM dNTPs,
221 0.2 µM for each forward and reverse primer, 0.025 units/µl OneTaq Polymerase
222 and 20-300 ng of template DNA. If crude DNA was used as a template, 3%
223 DMSO was added. PCRs were performed with the following Thermocycler
224 (Eppendorf) settings: 1 min at 94°C for initial denaturation, then 30-35 cycles of
225 30 s at 94°C (denaturation), 30 s at 45-65°C (annealing), 1 min/kb at 68°C
226 (extension) followed by 3-5 min at 68°C (final extension). Amplification of DNA
227 fragments for Gibson Assembly [58] was performed with Phusion High Fidelity
228 polymerase (ThermoFisher Scientific). Each reaction was set up as follows: 1×
229 Phusion HF buffer, 200 µM dNTPs, 0.5 µM of each forward and reverse primer,
230 0.02 U/µl Phusion polymerase and 20-300 ng of template DNA. PCRs were
231 performed with the following Thermocycler settings: 1 min at 98°C for initial
232 denaturation, then 30-35 cycles of 30 s at 98°C (denaturation), 30 s at 59-68°C
233 (annealing), 30 s/kb at 72°C (extension), followed by 3-5 min at 72°C (final
234 extension). Where long primers (>30 bp) were used, a 2-step PCR was

235 performed with the same reaction set up, but with different cycler settings: 1
236 min at 98°C for initial denaturation, then 5 cycles of 30 s at 98°C (denaturation),
237 30 s at 55°C (annealing), 30 s/kb at 72°C (extension), followed by 25 cycles of
238 30 s at 98°C (denaturing) and 30 s/kb at 72°C (extension). Subsequently the
239 reaction was incubated for 3-5 min at 72°C (final extension). PCR products
240 were purified using the Wizard SV Gel and PCR Clean-Up System (Promega).
241 Primers were sourced from Integrated DNA Technologies. Primer sequences
242 can be found in the Supplemental Table S2. Sequencing reactions were
243 performed using the Big-DyeTM Terminator Version 3.1 Ready Reaction Cycle
244 Sequencing Kit (Applied BioSystems, Carlsbad, California, USA), and
245 separated using an ABI3730 genetic analyser (Applied Bio Systems).
246 Sequence data was assembled and analysed using MacVector sequence
247 assembly software,
248 v14.5.2.

249 ## Preparation of constructs

250 The *gpiB* replacement construct, pBH1, was prepared as follows. Firstly, the
251 1,639 bp 5' and 1,389 bp 3' flanks of *gpiB* were amplified from wild type (WT)
252 *E. festucae* strain Fl1 genomic DNA by PCR using BH1/BH2 and BH3/BH4
253 primer pairs, respectively. The 1,394 bp hygromycin resistance cassette
254 (P*trpC-hph)* sequence was then amplified from pSF15.15 DNA using the
255 hph_F/hph_R primer pair. The 5,483 bp backbone vector, pRS426, was
256 amplified by PCR using the pRS426_F/pRS246_R primer pair. All PCRs were
257 performed with Phusion High-Fidelity DNA polymerase (NEB). The fragments
258 were then assembled via Gibson Assembly [58] and the correct assembly was

verified using a diagnostic restriction enzyme digest and sequencing. The replacement constructs for *sspM* (pBH2), *sspN* (pBH3) and *sspO* (pBH4) were generated in the same way. The 1,377 bp 5' and 1,333 bp 3' flanks of *sspM* were amplified with the BH11/BH12 and BH9/BH10 primer pairs, respectively; the 1,431 bp 5' and 1,433 bp 3' flanks of *sspN* were amplified with the BH15/BH16 and BH13/BH14 primer pairs, respectively; and the 1,443 bp 5' and 1,318 bp 3' flanks of *sspO* were amplified with the BH5/BH6 and BH7/BH8 primer pairs, respectively.

The *S. cerevisiae* complementation vector pSUC2T7M13ORI [52] was fully sequenced using primers BH25 to BH42 and BH61 to BH63. The nucleotide sequences encoding the secretion signals from SspN (54 bp), SspO (54 bp), SspM (54 bp) and GpiB (57 bp) were then amplified from *E. festucae* strain FI1 genomic DNA with the BH21/BH22, BH70/BH71, BH68/BH69 and BH64/BH65 primer pairs, respectively, using OneTaq polymerase. In doing so, these primers added a 5' *Eco*RI and 3' *Xho*I restriction site to each amplified sequence. Due to difficulties in working with small fragments different cloning strategies were effective for the different fragments. The *sspN* fragment was cloned into the TOPO-TA vector according to the manufacturer's instructions. Following this cloning step, pSUC2TM13ORI and the TOPO-TA vector containing the *sspN* secretion signal-encoding nucleotide sequence were digested with *Eco*RI and *Xho*I restriction enzymes and purified. The pSUC2TM13ORI vector backbone and secretion signal-encoding nucleotide sequence were then ligated using T4 ligase to generate pBH7. The *gpiB*, *sspM* and *sspO* secretion signal-encoding nucleotide sequences were directly digested with *Eco*RI and *Xho*I and purified, omitting the sub-cloning step into

284 the TOPO-TA vector. Subsequently the nucleotide sequences were then
285 directly ligated into *Eco*RI and *Xho*I digested pSUCTM13ORI generating pBH5
286 (*gpiB*), pBH11 (*sspM*) and pBH9 (*sspO*) respectively.
287 The four overexpression constructs were generated by Gibson
288 Assembly [58] of two fragments, respectively. The 2,844 bp backbone
289 fragment, containing a hygromycin resistance cassette, was amplified from
290 pBH12 with the primer pair BH75/76. The nucleotide fragments encoding *gpiB*,
291 *sspM*, *sspN* or *sspO* downstream of the P*tef* promoter as well as an ampicillin
292 resistance gene (*bla*) and an *oriT* were amplified from pBH14, pBH18, pBH21
293 or pBH24 respectively. For amplification, the primer pairs BH72/BH120 (3,476
294 bp), BH72/BH121 (3,725 bp), BH72/122 (3,525 bp) or BH72/BH123 (3,493 bp)
295 were used, respectively. Assembly of the respective fragments generated the
296 plasmids pBH29 (*gpiB*), pBH30 (*sspM*), pBH31 (*sspN*) and pBH32 (*sspO*).
297 Constructs encoding the genes of interest, C-terminally fused to an
298 8xHis tag, were generated via Gibson Assembly [58]. Again, each plasmid was
299 assembled from two fragments. The 2,488 bp backbone was amplified from
300 pBH30 using the BH176/BH75 primer pair. The forward primer, BH176, was
301 designed in a way that it added the 8xHis tag followed by a stop codon to the
302 fragment. The *sspM*-, *sspN*- and *sspO*- encoding fragments were amplified
303 from pBH30, pBH31 and pBH32 with the primer pairs BH72/BH177 (3,728 bp),
304 BH72/BH178 (3,528 bp) and BH72/179 (3,496 bp) respectively. The reverse
305 primers BH177/BH178/BH179 were designed in such a way that the stop codon
306 was removed and an overhang to the 8xHis tag was generated. The *gpiB*-
307 containing fragment was generated based on a previously generated construct,
308 pBH34. To prevent the loss of the 8xHis tag due to the addition of the GPI

309 anchor at the omega site [59], the 8xHis tag was added 30 bp upstream of the
310 omega site. To this end, the vector was assembled in two pieces amplified from
311 pBH34: the 2,823 bp fragment amplified by PCR with BH181/BH75 primer pair
312 containing the C-terminus of *gpiB* as well as the hygromycin resistance
313 cassette, and the 3,377 bp fragment amplified by PCR with the BH72/BH180
314 primer pair encoding an ampicillin resistance gene, an OriT and the *gpiB* N-
315 terminus. The primers BH180 and BH181 generated the 8xHis tag and thereby
316 overhangs with each other. This generated the plasmids pBH56 (*gpiB*), pBH57
317 (*sspM*), pBH58 (*sspN*) and pBH59 (*sspO*).

318 For the localization constructs, the plasmid pBV579 (PN4241) encoding
319 mCherry fused to a T-virus nuclear localization signal, was used [60]. The
320 constructs were generated via Gibson Assembly [58] from three different
321 fragments, generating C-terminal translational fusions between the *ssp* of
322 interest and mCherry-NLS separated by a (GGGS)x2 linker to facilitate
323 independent folding of the protein of interest and mCherry. All constructs
324 incorporated the native *ssp* promoter. The 5,060 bp backbone of the vector was
325 amplified by PCR from pBH12 with the BH76/BH78 primer pair. The 834 bp
326 mCherry-NLS fragment was amplified by PCR from pBV579 with the
327 BH79/BH80 primer pair, where the primer BH79 added the linker. The *sspM*,
328 *sspN* and *sspO* and the corresponding promoter encoding fragments were
329 amplified by PCR from WT genomic DNA using the primer pairs BH88/BH86
330 (827 bp), BH91/BH89 (977 bp) and BH93/BH94 (798 bp) respectively.
331 Assembly of the fragments generated the plasmids pBH19, pBH22 and pBH25.
332 All plasmids can be found in S2 Table and all primers in S3 Table.

Transformation of organisms

Chemically competent *E. coli* DH5α were transformed by heat-shock for 1 min at 42°C, followed by a 2 min incubation step on ice. Cells were allowed to recover for 1 h at 37°C in SOC medium and subsequently plated on LB agar containing ampicillin or kanamycin. *S. cerevisiae* YTK12 cells were made competent using the lithium acetate method [61], transformed by heat-shock for 30 min at 40°C [62] and plated on defined CMD tryptophan dropout medium (see above). *A. tumefaciens* GV3101 [63] cells were made competent and transformed by electroporation (25 mF, 2.5 kV, 200 Ω) [64]. Cells were allowed to recover in SOC medium and then plated on LB agar containing kanamycin. *E. festucae* Fl1 protoplasts were generated as previously described [65]. Protoplasts were transformed with up to 5 µg of the construct using the method previously described [66]. Protoplasts were allowed to regenerate overnight on regeneration agar (RG) and overlaid with RG agar containing either hygromycin B or geneticin the next day.

Protein extraction, protein purification and western blotting

For protein extraction, *E. festucae* strains were grown for at least 3 days in liquid PD at 22°C. Cultures were filtered through a nappy liner, washed, and snap frozen in liquid nitrogen and ground to a fine powder. Depending on the amount of mycelium, 400–800 µl of lysis buffer (50 mM NaH_2PO_4, 300 mM NaCl, 10 mM imidazole, 0.1% (v/v) IGEPAL CA360, 0.2 mM PMSF, 10 µl/ml protease inhibitory cocktail (Sigma Aldrich), 5 mM β-mercaptoethanol) was

added and samples were vortexed for 10 min. Subsequently, samples were centrifuged at 14,000 g for 15 min at 4°C and the supernatant was stored at -20°C. The growth medium of each strain (50–80 ml) was collected and filtered through a 0.45 µm filter. Samples were concentrated to approx. 2 ml with Vivaspin 20 MWCO 30,000 spin columns (GE Healthcare Life Sciences) according to the manufacturer's instructions and washed twice with 10 ml lysis buffer. Samples were stored at -20°C.

The protein purification was performed with Ni-NTA spin columns (Qiagen) according to the manufacturer's instructions with the exception of the elution buffer (50 mM NaH_2PO_4, 300 mM NaCl, 10–500 mM imidazole, 0.1% (v/v) IGEPAL CA360), 0.2 mM PMSF, 10 µl/ml protease inhibitory cocktail (Sigma Aldrich)). Samples were loaded onto 15% (w/v) SDS polyacrylamide gels, electrophoresed at 100 V for 1.5 h then electrophoretically transferred at 30 V for 1 h to PMSF membranes (Roche). The primary antibody, rabbit α-His (Abcam, ab9108), was used in a 1:2,000 dilution and the secondary goat α-rabbit-HRP (Abcam, ab6721) in a 1:10,000 dilution. Detection was performed with the Amersham ECL western blotting detection reagent (GE Healthcare Life Sciences).

For the verification of Ssp and GpiB production in *N. benthamiana*, total protein was extracted from the infiltrated area. First the tissue was snap frozen, then ground to a fine powder in liquid nitrogen and subsequently resuspended in an equal volume of GTEN buffer (10% glycerol, 100 mM Tris pH 7.5, 1 mM EDTA, 150 mM NaCl, 10 mM DTT, 0.2% IGEPAL CA360, 10 µl/ml protease inhibitory cocktail (Sigma Aldrich), 1% PVP). Afterwards, samples were centrifuged at 14,000 rpm for 15 min at 4°C and the supernatant was stored at

382 -20°C. Samples were loaded onto a 15% SDS polyacrylamide gel and
383 transferred onto PMSF membranes (Roche) as described above. The primary
384 antibody, a mouse α-FLAG antibody (Sigma, F6165), was used in a 1:2,000
385 dilution followed by the secondary goat α-mouse–HRP (Santa Cruz
386 Biotechnology, Dallas, TX, USA) antibody in a 1:1,000 dilution.
387

388 RNA extraction and qPCR

389 For the determination of the gene copy number, high quality gDNA was
390 extracted as described above and qPCR was performed with SYBR Green
391 (Invitrogen) on a LightCycler 480 System (Roche) as per the manufacturer's
392 instructions. Each sample was analysed with two technical replicates. The
393 single copy genes *hepA* (EfM3.043690) and *pacC* (EfM3.009480) were used
394 as reference genes and the copy number was calculated relative to WT as
395 described previously [67].
396 For the determination of relative expression levels, RNA was extracted
397 from freeze-dried mycelium using TRIzol reagent (Invitrogen). Subsequently,
398 cDNA synthesis was performed with the QuantiTect Reverse Transcriptase kit
399 (Quiagen). The qRT-PCR was performed as described above. Each sample
400 was analysed with two technical replicates. The genes coding for translation
401 elongation factor 2 (EF-2, EfM3.021210) and 40S ribosomal protein S22 (S22,
402 EfM3.016650) were chosen as reference genes as previously described [68].
403 The expression level was calculated relative to WT as described previously
404 [67]. All primers used for qPCR and qRT-PCR can be found in the S3 Table.
405

406 ## Analysis of transmission of *E. festucae* mutants into *L.*

407 ## *perenne* seeds

408 Twenty endophyte free seedlings of *L. perenne* cv. Samson were inoculated
409 with three independent deletion strains of *gpiB* (T111, T133, T148), *sspM* (T52,
410 T99, T163), *sspN* (T10, T30, T52) and *sspO* (T78, T195, T210) [56, 69]. Twenty
411 seeds were inoculated with PD agar as mock control. Plants were grown in root
412 trainers in the greenhouse for 7 weeks at 20°C with a photoperiod of 16 h of
413 light and tested for presence of the endophyte by immunoblotting [70]. Five
414 immunoblot positive plants of each strain were transferred to new pots 10
415 weeks post-infection and grown in the greenhouse for additional two weeks.
416 For vernalisation, plants were transferred to a growth cabinet and cultivated for
417 7 weeks at 6°C with a short-day photoperiod of 8 h light and 16 h dark. Starting
418 from four weeks until ten weeks after vernalisation, plants produced
419 inflorescences. Ovaries were collected, stored in 95% EtOH and stained [69]
420 when pollen was visible and ovaries mature. Stained ovaries were stored in
421 70% glycerol until microscopic observation. Seeds were collected, dried and
422 stored in the fridge until further use. For microscopy and immunoblotting of
423 seeds, the seeds were surface sterilised [56, 69], germinated on wet filter paper
424 overnight and cross sections used for immunoblotting.
425

426 ## Microscopy

427 For microscopy of *E. festucae* culture growth, a small piece of a fresh colony
428 was inoculated on the edge of a glass slide covered with a thin layer of 1.5%
429 H_2O agar placed on an agar plate with 3% H_2O agar. Strains were incubated

for 6 days before examination with an Olympus IX71 inverted fluorescence microscope using the filter sets for DIC and CFW/DAPI. For staining of the cell wall, a drop of a 3 mg/ml of Calcoflour White was added to the sample just before microscopy.

For the examination of growth and morphology of hyphae *in planta*, pseudostem tissue was stained with aniline blue diammonium salt (Sigma) and Wheat Germ Agglutinin conjugated to AlexaFluor®488 (WGA-AF488, Molecular Probes/Invitrogen). First, infected tissue was incubated in 100% EtOH overnight at 4°C followed by an incubation in 10% KOH overnight at 4°C. Samples were washed at least 3 times with PBS (pH 7.4) before incubation in the staining solution (0.02% aniline blue, 10 ng/ml WGA-AF488, 0.02% Tween®-20 (Invitrogen) in PBS (pH 7.4)) for 10 min. Samples were vacuum-infiltrated with the staining solution for 30 min and then stored at 4°C until analysis. Examination of these samples was performed with a Leica SP5 DM6000B confocal microscope (488 nm argon and 561 nm DPSS laser, 40× oil immersion objective, NA= 1.3) (Leica Microsystems). For TEM pseudostem samples were fixed with 3% glutaraldehyde and 2% formaldehyde in 0.1 M phosphate buffer, pH 7.2 for 1 h, as described previously [71]. The fixed samples were examined with a Philips CM10 TEM and the images were acquired using a SIS Morada digital camera. Sections of the resin-embedded samples were also stained with 0.05% toluidine blue in phosphate buffer and heat-fixed at approx. 100°C for 10 s. These samples were examined with a Zeiss Axiophot Microscope with Differential Interference Contrast (DIC) Optics and Colour CCD camera.

For the *in planta* localization of the Ssp-mCherry-NLS fusion proteins, un-fixed pseudostem samples were examined with a Leica SP5 DM6000B confocal microscope (488 nm argon and 561 nm DPSS laser, 40× oil immersion objective, NA= 1.3).

Preparation of binary vectors, agroinfiltration and suppression assay

All binary backbone vectors for transformation into *Agrobacterium* are listed in S2 Table. The plasmids pBH44-47 were generated via Golden Gate cloning using pICH86988 as the backbone. The nucleotide sequences of *gpiB, sspM, sspN and sspO* were amplified by PCR without their native secretion signal from WT *E. festucae* cDNA with primer pairs adding additional base pairs for the necessary overhang and a *Bsa*I restriction site (*gpiB*: BH165/BH166, *sspM*: BH167/BH168, *sspN*: BH170/BH171, *sspO*: BH172/BH173) as described. The *N. tabacum* secretion signal PR1α was obtained from pUC19B (S. Marillonet, pers.comm.). The digestion and ligation were conducted either in one step or in two separate steps. The one-step reaction was performed in a total volume of 20 µl with 1 µl T4 ligase (NEB) and 1 µl BSA (NEB) and equimolar amounts of all three inserts (approx. 50 ng total). The reaction was performed in a Thermocycler (Eppendorf) with the following settings: 25 cycles of 37°C for 3 s and 16°C for 4 s, followed by 5 s inactivation at 50°C and 80°C each. For the two-step reaction, the digest was performed in a volume of 10 µl with 1 µl BSA (NEB) and equimolar amounts of each insert. The reaction was performed at 37°C for 3 h. Subsequently the reaction was inactivated by heating to 50°C. For the ligation, the volume was topped up to 20 µl per reaction including 1 µl T4

ligase (NEB). The reaction was incubated at 16°C in a Thermocycler (Eppendorf) overnight followed by an 80°C inactivation step. A diagnostic restriction digest and DNA sequencing confirmed the sequence of all vectors. Electro-competent *A. tumefaciens* GV3101 cells were generated and transformed as described. Cells were allowed to recover in SOC medium and subsequently plated on LB agar containing kanamycin. To perform the infiltrations, fresh strains were inoculated in 3 ml LB medium with kanamycin and incubated at 30°C overnight. The next day, cultures were spun down and resuspended in 1 ml infiltration buffer (10 mM $MgCl_2$, 10 mM MES-KOH, 100 µM acetosyringone). These cultures were adjusted to an OD_{600} of 0.4 in the necessary amount of infiltration buffer (usually 5–10 ml) and incubated at room temperature for at least 3 h before infiltration. To confirm the expression of each of the constructs, total protein was extracted from infiltrated *N. benthamiana* tissue and a western blot was performed.

For HR suppression assays *A. tumefaciens* strains carrying plasmids encoding the potential suppression gene pBH44 (*gpiB*), pBH45 (*sspM*), pBH46 (*sspN*), pBH47 (*sspO*), pBIN-Plus-Avr3a (suppression control), pICH86966-N-3xFlag-GFP (control), pBC302-3-R3a (HR control) were infiltrated 24h before infiltration with pBC302-3-INF1 and pBIN-Plus-Avr3a (HR control).

Results

Candidate effectors of *E. festucae*

The recent availability of the complete telomere-to-telomere genome sequence of *E. festucae* strain Fl1, which is 35 Mb in size and encodes 8,465 predicted genes on seven chromosomes [26], provided us with the opportunity to study the organization, structure and genome context of genes encoding candidate effector proteins. First, we established which of the 8,465 predicted genes likely encode secreted proteins. For this purpose, we defined a secreted protein as any protein with a predicted amino N-terminal secretion signal, as determined using the SignalP server, that targets the protein outside of the fungal plasma membrane [44]. This definition does not exclude those proteins with a predicted transmembrane domain or GPI anchor modification site. In total, 682 genes (8.1%) were predicted to encode a secreted protein. We then analysed which of the 682 predicted secreted proteins encode candidate effectors using the EffectorP server, which predicts effectors using a machine learning approach [41]. In addition, we applied a size cutoff of ≤200 amino acids, as most fungal effectors fall within this range [72]. Out of 175 predicted secreted proteins meeting this length requirement, 141 were predicted to be candidate effectors by EffectorP. For subsequent analyses the 8,465 predicted proteins were subdivided into 'effector candidates' (n=141), 'secreted', comprising all putatively secreted proteins that are not classified as effector candidates (n= 541), and 'non-secreted' made up of all putatively non-secreted proteins (n= 7,783) (S4 Table).

To gain further insight into the possible functions of the 141 effector candidates, and to determine which of these predicted proteins have homologs across the *Sordariomycetes*, a BLASTp analysis was performed against fungal reference proteins at NCBI. Of the 141 effector candidates, 83 were found to

525 have sequence homology to proteins present in the NCBI database (E-value
526 cut off of ≤1e-10), but 56 of these were to uncharacterized or hypothetical
527 proteins. Among the 'hits' to characterized proteins were ten cell wall-
528 associated proteins, including hydrophobins and carbohydrate-binding
529 proteins, two toxins and other small secreted proteins (S4 Table). The majority
530 of 'hits' were to proteins from species in the Hypocreales (21 *Claviceps spp*.,
531 21 *Metarhizium spp*., 14 *Pochonia spp*., 6 *Moelleriella spp*., 6 *Ustilaginoiea*
532 *spp*.), with the remaining hits to proteins from other species within the
533 Sordariomycetes. For 58 of the effector candidates, no homologs could be
534 identified (E-value>1e-10), but analysis against a custom made Clavicipitaceae
535 endophyte database (epichloe.massey.ac.nz)[47] found potential homologs for
536 20 of these proteins. The remaining 38 Ssps are apparently unique to *Epichloë*
537 *spp.* (S4 Table).

538 Given many fungal effectors are cysteine-rich, a property that enables
539 the formation of disulfide bonds and protein folding to maintain structural
540 integrity in the protease-rich apoplast [73, 74], the frequency of cysteine
541 residues in the effector candidates was compared with that of the secreted and
542 non-secreted categories. As expected the candidate effectors were significantly
543 more cysteine-rich (3.6% of residues) than either secreted (frequency= 1.7%,
544 *P*= <1e-18) or non-secreted (frequency= 1.4%, *P* < 1e-18) (S1 File).

545 In smut fungi, secreted genes are predominantly arranged in clusters
546 within the genome and are highly upregulated during tumor formation [75, 76].
547 We therefore tested whether the genes encoding the *E. festucae* effector
548 candidates were clustered by mapping them to each of the seven
549 chromosomes (Fig 1A). From this low-resolution analysis, it appears that the

genes encoding effector candidates of *E. festucae* are evenly distributed throughout the genome. This conclusion was supported by an analysis comparing the within category gene distances, which concluded that genes encoding effector candidates are not clustered in the *E. festucae* genome (Fig 1A). Of all the genes encoding candidate effectors, only eight (four gene pairs) were found within 1 kb of each other. In fact, the mean distance between candidate effector genes was not significantly different from that expected from a random subset of the 141 genes (P= 0.236).

E. festucae is one of several filamentous fungi that has a genome comprised of distinct gene-poor AT isochores and gene-rich GC isochores [21, 26]. Because the AT-rich regions are subject to an unusually high mutation rate [77-80] they are frequently referred to as 'birthplaces' for new genes such as those encoding effectors and secondary metabolites [81]. In *Leptosphaeria maculans* 20% of all genes in AT isochores encode small secreted proteins (SSPs, effector candidates), whereas they make up just 4.2% of all genes in GC isochores [21]. In contrast to *L. maculans*, there was no enrichment of genes encoding effectors in or near to AT isochores of the *E. festucae* genome (P= 0.369) (Fig 1B). Similarly, there was no enrichment of genes in the secreted category in AT isochores (P= 0.812) (Fig 1B). Indeed, of the 548 genes located in or within 1,000 bp of an AT isochore, only 1.5% and 4.7% encoded a protein from the candidate effector and secreted categories, respectively.

Given some fungal effector genes, such as the *AVR-Pita* gene from *Magnaporthe oryzae* [82], are found in close proximity to telomeres, we took advantage of the telomere-to-telomere *E. festucae* genome sequence to determine if genes encoding candidate effectors are located close to telomeres.

These regions of the genome are also subject to higher mutation rates than the remainder of the genome and potential sites for the evolution of environment adaptation genes such as those encoding effectors [83, 84]. However, genes encoding effector candidates were not significantly closer to telomeres than other genes present in the *E. festucae* genome ($P< 0.787$) (Fig 1C).

Transposable elements are increasingly seen as important regulators of gene expression [85, 86], and miniature inverted-repeat transposable elements (MITES) have been postulated to play a role in the expression of *E. festucae* genes *in planta* [24, 26]. For this reason, the distance between genes encoding effector candidates and MITES was analyzed in the *E. festucae* genome. This analysis revealed that genes encoding effector candidates are more likely to contain a MITE within 2 kb of their transcription start site than non-secreted proteins ($P= 3.56e-18$, Fig 1D). Genes encoding other secreted proteins were also more likely to contain a MITE immediately upstream of their transcription start site than non-secreted proteins ($P= 1.66e-7$). No particular MITE family is over-represented within 2 kb of these genes.

Apart from the physical organization of effector genes within fungal genomes, the expression of these genes often follows distinct host colonization patterns and are generally more highly expressed *in planta* than in axenic culture [72, 87, 88]. We therefore analysed the transcript expression profiles of the three different gene categories between *E. festucae* grown *in planta* and in axenic culture. Genes encoding effector candidates were significantly more highly expressed *in planta* (mean $\log_2$ fold difference= 1.20, $P< 2e-16$) (Fig 2A). Other secreted proteins were also moderately more highly expressed *in planta* (mean $\log_2$ fold difference= 0.20, $P= 0.004$) (Fig 2A).

Given genes encoding effector candidates are preferentially silenced in axenic culture compared to *in planta* we examined whether this might be due to the chromatin state as shown for *L. maculans* where RNAi-induced silencing of DIM-5, a histone H3 lysine 9 trimethyl transferase, and heterochromatin protein 1 (HP1), led to de-repression of effector gene expression in axenic culture [89]. We therefore compared expression of *E. festucae* genes encoding effector candidates in a *hepA* (homolog of *HP1*) mutant versus wild type. We found candidate effector genes were moderately more highly expressed in the *hepA* mutant (mean $\log_2$ fold difference= 0.310, P= 4.13e-9) (Fig 2B). For some genes, this change in gene expression was substantial. Eleven percent of putative effectors showed $\log_2$ fold difference in expression greater than 2, a significantly higher proportion than observed in larger secreted (1.5% of genes, P= 5e-14) or non-secreted proteins (3% of genes, P= 1e-4)).

Previously we showed that disruption of the usually asymptomatic interaction between *L. perenne* and *E. festucae* by infecting the host with symbiotic mutants of *E. festucae* results in major changes in the fungal transcriptome [47]. We therefore tested whether effector candidate gene expression changed in the Δ*sakA*, Δ*noxA,* Δ*proA* and Δ*hepA* symbiotic mutants using previously generated transcriptome data sets [47](Tetsuya & Scott, personal communication). Generally, genes encoding effector candidates were upregulated in each of the dysfunctional interactions (mean difference of 0.411 log2 fold units, P = 5.28 x 10-8) (Fig 2C). A closer investigation showed that ten genes encoding effector candidates SspB-SspK were consistently upregulated across all four different mutant interactions and three genes encoding effector

624 candidates SspM-SspO were consistently down regulated [47](Tetsuya &
625 Scott, personal communication).

626 In summary, the genes encoding effector candidates from *E. festucae*
627 do not show a distinct distribution pattern as has been described for some other
628 fungi, but seem to be evenly dispersed throughout the genome. These genes
629 do not cluster, and are not preferentially located in AT-rich isochores or
630 telomeres. However, these genes are enriched with respect to their proximity
631 to MITES. As found for many other fungi, a significant number of genes
632 encoding effector candidates from *E. festucae* are preferentially upregulated *in*
633 *planta*. Furthermore, many of these genes are upregulated in symbiotic mutants
634 of *E. festucae* that disrupt the restrictive pattern of growth observed for WT *E.*
635 *festucae*.

636
637

638 **Fig 1. Physical properties of genes encoding effector candidates in *E.***
639 ***festucae*.**
640 (A) Location of genes encoding effector candidates (black circles) on the seven
641 chromosomes of *E. festucae* strain Fl1. The blue line indicates AT richness in
642 a 1,000 bp window. (B) Distance of each *E. festucae* gene from AT-rich regions
643 (isochores). (C) Distance of each *E. festucae* gene from telomeres. (D)
644 Distance of each *E. festucae* gene from MITES. Genes are divided into the
645 categories 'non-secreted' (n= 7783), 'secreted' (n= 541) and 'effector
646 candidates' (n= 141).

647

648 **Fig 2. Analysis of gene expression in WT *E. festucae* and symbiotic**
649 **mutants of *E. festucae* grown**. (A) Log_2 fold difference in gene expression

650 between WT *E. festucae* grown *in planta* and in culture. (B) Log_2 fold difference
651 in gene expression between WT and a *hepA* deletion strain grown in culture.
652 (C) Log_2 fold difference in gene expression between WT and Δ*noxA,* Δ*proA,*
653 Δ*sakA* and Δ*hepA* strains grown *in planta*. Number of genes in each category:
654 'non-secreted', n= 7783; 'secreted', n= 541; and 'effector candidates', n= 141.
655

656 Sequence analysis of downregulated effector candidates

657

658 To gain further insight into the role of *E. festucae* effectors in the symbiotic
659 interaction with *L. perenne*, the three genes described above (*sspM*,
660 EfM3.016770; *sspN*, EfM3.062700; and *sspO*, EfM3.014350) that were found
661 to be downregulated in all four symbiotic mutant interactions, were selected for
662 genetic analysis [47](Tetsuya & Scott, personal communication). The fact that
663 they were among the top 100 genes upregulated *in planta* compared to axenic
664 culture was an additional criterium for selecting these three genes (Fig 2A, S4
665 Table). A fourth gene, *gpiB* (EfM3.018200), encoding a putative GPI-anchored
666 protein, was also selected for functional analysis because it had an identical
667 expression profile to *sspM*, *sspN* and *sspO* [47], and because GPI-anchored
668 proteins are known to have important roles in fungal virulence [42, 43].
669 cDNA sequencing confirmed that the proposed gene models for each of
670 these four genes were correct. In the case of *sspN*, where two alternatively
671 spliced forms were proposed the second of these (mRNA-2) corresponded to
672 the cDNA sequence. The *gpiB* gene (EfM3.018200) is predicted to encode a
673 protein of 126 aa with an unmodified MW of 12.61 kDa (8.7 kDa without

674 secretion signal and C-terminus beyond the omega cleavage site), while the
675 *sspM* gene (EfM3.016770) is predicted to encode a protein of 177 aa with an
676 unmodified MW of 18.87 kDa (17.1 kDa without secretion signal). The protein
677 encoded by *sspN* (EfM3.062700) is predicted to be 127 aa in length with an
678 unmodified MW of 14.98 kDa (13.19 kDa without secretion signal), while the
679 protein encoded by *sspO* (EfM3.014350) is predicted to be 104 aa in length
680 with an unmodified MW of 11.11 kDa (9.4 kDa without secretion signal) (Fig 3).
681 Analysis of the selected protein sequences with InterproScan [90],
682 SMART [91], T-Reks [92] and HHPRED [93] did not identify any conserved
683 domains with known function, but did predict a number of different structural
684 features and secondary modifications (Fig 3). GpiB contains a predicted *N*-
685 glycosylation motif as well as a putative C-terminal GPI anchor. The SspM
686 protein contains a possible pre-pro domain ending with a classical LxKR kexin
687 cleavage site motif and a predicted *N*-glycosylation site. SspN is a repeat-
688 containing protein, consisting of 7.5 almost perfect repeats of 15 aa. Like SspM,
689 it also contains a putative kexin cleavage site. Analysis of the SspO sequence
690 did not reveal any obvious structural features. Both SspM and SspO are rich in
691 cysteines; SspO containing eight and SspM containing six downstream of the
692 cleavage site, whereas SspN and GpiB are cysteine-free (Fig 3).
693 A BLASTn analysis of the four selected genes revealed a patchy
694 distribution within the *Epichloë* species, with only *gpiB* present in all analyzed
695 genomes available on the Kentucky Endophyte Database [94]. The observed
696 distribution patterns did not correlate with specific hosts or the sexual
697 phenotype of the fungus (S5 Table). Alignment of the protein sequences of
698 interest with the corresponding homologs in other *Epichloë* species showed

699 that GpiB and SspO are highly conserved (S1A and S1D Figs). Interestingly,
700 SspM was highly conserved from the N-terminus to the proposed kexin
701 cleavage site and less conserved beyond this site (S1B Fig). The repeat
702 structure of SspN was also conserved, with homologs mainly differing in their
703 number of repeats (S1C Fig). A BLASTp analysis identified homologs of Ssps
704 and GpiB in species outside of *Epichloë* (S4 Table); however, none of these
705 are functionally characterized.
706
707 **Fig 3. Schematic representation of the small secreted proteins SspM,**
708 **SspN, SspO (effector candidates) and the GPI-anchored protein GpiB and**
709 **their corresponding genes.** GpiB (EfM3.018200) is encoded by a 381 bp
710 gene that lacks introns, and is predicted to encode a protein of 126 aa. The
711 gene encoding the predicted 177 aa SspM (EfM3.016770) is 630 bp in size and
712 contains one intron. SspN (EfM3.062700) is encoded by a gene of 430 bp, with
713 one intron, and encodes a predicted protein of 127 aa. SspO (EfM3.014350) is
714 encoded by a 398 bp gene, containing one intron, and is predicted to be encode
715 a protein of 104 aa. N-terminal secretion signals (SS) are indicated by blue
716 boxes and post-translational modifications and structural motifs by pink bars
717 (*N*-glycosylation), grey bars (GPI anchor modification site), facing arrows
718 (protease cleavage site), hollow ovals (repeats) and small black bars (cysteine
719 residues).
720

721 GpiB, SspM, SspN and SspO are secreted

722 To experimentally verify secretion of the three selected candidate effectors and
723 the GPI anchored protein, GpiB, a complementation assay was performed in

724 *S. cerevisiae*. The nucleotide sequence encoding the secretion signal predicted
725 by SignalP was ligated in frame to the N-terminus of the *S. cerevisiae* invertase
726 *SUC2* encoded on the pSUC2T7M13ORI vector [52]. These constructs were
727 then transformed into the *SUC2*-negative yeast strain YTK12 and tested for
728 growth on CMDRAA medium, which contains raffinose as the sole carbon
729 source. All four test strains expressing the secretion signal-Suc2 fusion protein
730 grew on this medium whereas the strain expressing Suc2 without a secretion
731 signal and the untransformed YTK12 did not (Fig 4). These results indicate that
732 the signal peptides of SspM, SspN, SspO and GpiB are sufficient to mediate
733 secretion in *S. cerevisiae*.
734
735 **Fig 4. Analysis of the GpiB, SspM, SspN and SspO secretion signals in a**
736 ***S. cerevisiae* complementation assay.** YTK12 strains transformed with
737 pSUC2T7M13ORI encoding *SUC2* transcriptionally fused to *gpiB, sspM, sspN*
738 or *sspO* secretion signal nucleotide sequence, as well as the empty vector and
739 YTK12-only controls. Only strains expressing the secretion signal-Suc2 fusion
740 proteins were able to grow on defined medium with raffinose as carbon source
741 (CMDRAA). SS, secretion signal. All strains grew on the control plates
742 containing YPDA media.
743

744 Analysis of secretion and processing of GpiB, SspM, SspN
745 and SspO in *E. festucae*

746 As discussed above, many effectors are post-translationally processed (e.g. by
747 proteolytic cleavage) or modified (e.g. by glycosylation) to their final form. To
748 verify the secretion of these proteins in *E. festucae*, and to check if they are

749 modified (Fig 3), His-tagged fusions of GpiB, SspM, SspN and SspO were
750 purified from extracts of *E. festucae* mycelia (intracellular form), as well as from
751 the liquid culture medium (extracellular form), separated by PAGE and
752 analyzed by western blotting (Fig 5). All four proteins were present in extracts
753 from fungal mycelia. The 13 kDa band for GpiB is larger than the predicted His-
754 tagged size of 9.8 kDa, possibly due to the addition of the GPI anchor and/or
755 modification by *N*-glycosylation. A band corresponding to SspN was detected
756 at approx. 14 kDa, which agrees with the predicted His-tagged size of 14.31
757 kDa for the unprocessed protein, indicating that under the growth conditions
758 used, this protein is not cleaved, even though it has a predicted kexin cleavage
759 site. The signal for SspO was very faint, and slightly larger (12 kDa) than the
760 predicted His-tagged size of 10.5 kDa for this protein. In contrast, two bands of
761 20 and 16 kDa were detected for SspM, with the band of higher molecular
762 weight being very faint. SspM has a predicted His tagged size of 18.22 kDa in
763 the unprocessed form (with its predicted pro-domain) and 12.7 in the cleaved
764 form (without its predicted pro-domain). Taking into account a probable
765 increase in size due to the predicted *N*-glycosylation, the sizes observed for
766 SspM agrees with the predicted sizes of the kexin-unprocessed and processed
767 forms, respectively. The presence of additional bands on the western is
768 probably the result of non-specific binding to other proteins present in the crude
769 extract separated on these gels.

770 Analysis of the culture medium identified bands for SspO and SspM, but
771 the latter was only detected when the culture medium was buffered to pH 6.5
772 with 50 mM HEPES. The bands detected for SspO and SspM were the same
773 size as those seen in the mycelial fraction, with the latter again present as a

774 double band. These results suggest that SspO does not contain any secondary
775 modifications and is secreted into the culture medium, whereas SspM is
776 processed at the predicted kexin site. The absence of bands for GpiB and SspN
777 in the culture medium suggest that these proteins are either unstable in the
778 culture medium or remain attached to the fungal hyphae following secretion.
779
780 **Fig 5. Western blot analysis of GpiB-His, SspM-His, SspN-His and SspO-**
781 **His extracted from *E. festucae* mycelia and culture medium.** Genes of
782 interest (*gpiB*, *sspM*, *sspN* and *sspO*) were translationally fused to an 8x His
783 tag at the C-terminus and constructs were placed under the control of the P*tef*
784 overexpression promoter. Total protein was extracted from fungal mycelia and
785 the corresponding growth medium, and His-tagged proteins purified on Ni-NTA
786 spin columns eluted with increasing concentrations of imidazole. Samples were
787 separated on a 15% SDS PAGE gel, transferred to membranes and probed
788 with an anti-His antibody. SspM-His was extracted from *E. festucae* strains
789 grown in medium buffered to pH 6.5 with 50 mM HEPES. Predicted sizes of
790 proteins were calculated on the basis that each protein lacked the secretion
791 signal and had the 8x His-tag.
792

793 Functional analysis of *gpiB, sspM, sspN and sspO*

794
795 To investigate whether *sspM*, *sspN*, *sspO* or *gpiB* are necessary for
796 establishing a mutualistic symbiotic interaction, given their expression is
797 downregulated in three different symbiotic mutants [47], each gene was
798 individually deleted in the WT background using a gene replacement approach.

Replacement constructs, pBH1–4, were prepared, and PCR-amplified linear fragments of each were transformed into WT protoplasts. Putative gene replacements were identified by PCR screening approx. 200 independent Hyg^R transformants with primers that flank the site of *hph* integration. Additional PCR screening with primer sets that amplify the left and right flanks of each of the insertion sites was used to confirm the transformants selected had gene replacements. Southern blot analysis of genomic DNA extracted from these strains identified three independent deletion strains for *gpiB* (T111, T133, T148), *sspM* (T52, T99, T163*) sspO* (T78, T195, T210), and *sspN* replacement (T10, T30, T52) (S2 Fig).

To determine the phenotype of the deletion strains in culture, the whole colony morphology of each independent deletion strain was compared to that of WT, which is typically circular with white fluffy mycelium that thins and flattens towards the edges. This comparison revealed that the whole colony morphology of each deletion strain was indistinguishable from WT (Fig 6). Given this result, the hyphal morphology was more closely analysed by microscopy. *E. festucae* WT had smooth hyphal tips with hyphae arranged in bundles that are thicker in the more mature inner zone of the colony. Hyphae of WT had hyphal bridges, which are formed by tip-to-side fusion [40], as well as hyphal coil structures, which are thought to promote conidiophore formation [40]. When stained with Calcofluor white, which preferentially binds to chitin, the cell walls of WT hyphae uniformly fluoresced. Similar to the whole-colony comparison, each of the deletion strains had an indistinguishable phenotype to that of WT, forming hyphal bundles, with occasional hyphal fusion, and coil formation (Fig 6).

To determine the host interaction phenotype, strains were inoculated into *L. perenne* seedlings and the phenotype of infected plants examined eight weeks post-planting. At this time point, WT infected plants typically have 2–6 tillers that are up to 50 cm in length (Fig 7). Plants infected with the deletion mutants had the same interaction phenotype as those infected with WT, with no statistically significant difference in either the number or length of tillers (Fig 7). To analyse the cellular phenotype of the infected plants, pseudostem cross sections were fixed and embedded in resin, and slices stained with Toluidine blue. WT-infected samples typically have one to two hyphae per intercellular space and never colonize the vascular bundle tissue (Fig 8). The mutant-infected plants had the same cellular phenotype as WT plants, with one to two hyphae per intercellular space and no hyphae within the vascular bundles (Fig 8). Given these results, samples were then prepared for TEM, to give better resolution of the cellular phenotype. The cellular structure of tissue infected with *E. festucae* mutants was indistinguishable from WT (Fig 8). In addition, longitudinal leaf sections were infiltrated with wheat germ agglutinin, a chitin-binding lectin, conjugated to AlexaFluor 488 (WGA-AF488), as well as aniline blue, a β-glucan-binding dye, and analysed by confocal laser scanning microscopy (CLSM). Leaves infected with WT typically had one hypha (red pseudocolor, aniline blue) with regularly spaced septa (blue pseudocolor, WGA-AF488) growing between plant cells (Fig 9). These hyphae occasionally branched and where tips of branches meet, fused to establish a hyphal network throughout the leaf tissue (Fig 9). The morphology and growth pattern of the mutant hyphae were indistinguishable from WT (Fig 9).

848 Next we tested whether these mutants could be vertically transmitted
849 into the seeds of *L. perenne*. Plants infected with each of the individual
850 transformants were vernalized and ovaries collected from flowers for CLSM and
851 seed collected from mature inflorescences to test for endophyte in each of
852 these tissues. Endophyte was shown to be present in ovaries of some of the
853 flowers collected from plants infected with Δ*gpiB*, Δ*sspM* and Δ*sspN* mutants
854 but not Δ*sspO* (S3 Fig; S6 Table). Seeds of Δ*gpiB* (2/43), Δ*sspM* (25/90) and
855 Δ*sspN* (14/70) were immunopositive indicating that these three mutants were
856 vertically transmitted (S6 Table). However, none of the seeds infected with
857 Δ*sspO* (0/60) were found to contain endophyte suggesting this mutant was
858 unable to be transferred to the seed.

859 In summary, deletion of *gpiB*, *sspM* and *sspN* does not result in any
860 obvious culture or plant interaction phenotype, suggesting that the proteins
861 encoded by these genes are not essential for any of these growth processes.
862 Similarly, *sspO* appears to be dispensable for most of these growth processes
863 but may be important for vertical transmission within the host grass.

864

865 **Fig 6. Culture phenotype of WT and deletion mutant strains.** (A)-(D)
866 Representative DIC images captured with the inverted microscope of WT and
867 deletion mutant strains grown on 1.5% water agar for 6 days. (A) Hyphal bundle
868 formation. (B) Hyphal fusion points. (C) Hyphal coils. (D) Hyphal tips. (E)
869 Hyphae stained with Calcofluor white to examine cell wall composition. (F)
870 Colony morphology of WT compared to the deletion strains grown on 2.4% PDA
871 for 7 days. Bar: 20 μm.

872

873 **Fig 7. Plant phenotype of *L. perenne* infected with *E. festucae* WT and**
874 ***gpiB, sspM, sspN* and *sspO* deletion mutant strains.** (A-D) Whole plant
875 phenotype of WT and deletion mutant-infected *L. perenne* plants 8 weeks post-
876 planting. (E and F) Box plots representing tiller number (E) and length (F) of
877 ryegrass plants 8 weeks post-planting infected with *E. festucae* WT (n=6) and
878 Δ*gpiB* (n=9/9/5), Δ*sspM* (n=10/15/13), Δ*sspN* (n=13/8/8) and Δ*sspO* (n=7/8/9)
879 mutant strains. One-way ANOVAs were used to test for differences in both plant
880 phenotypes between wildtype and modified strains. In each case the ANOVA
881 was fitted with R and a Bonferroni correction was applied to all p-values to
882 account for multiple testing.
883
884 **Fig 8. Light microscopy and transmission electron micrographs of the *in***
885 ***planta* cellular phenotype of *E. festucae* WT and *gpiB, sspM, sspN* and**
886 ***sspO* deletion mutant strains.** (A) Light microscope analysis of fixed *L.*
887 *perenne* pseudostem cross sections stained with Toluidine blue. The focus of
888 the section is on the vascular bundles and surrounding regions; Bar= 10 µm.
889 (B) TEM analysis of hyphal growth in the host apoplast; Bar= 2 µm. (C)
890 Magnified transmission electron micrograph of one single hypha; Bar= 1 µm.
891 Representative images from one of the independent mutants for each gene.
892 Red arrows indicate position of hyphae and green arrows epiphyllous hyphae.
893
894 **Fig 9. Confocal depth series images of *in planta* cellular phenotype of *E.***
895 ***festucae* WT and *gpiB, sspM, sspN and sspO* deletion mutant strains.**
896 Infected *L. perenne* pseudostem samples were stained with aniline blue/WGA-
897 AF488. Hyphae show aniline blue fluorescence of β-glucans (red pseudocolor)

and chitin staining of septa with WGA-AF488 (blue pseudocolor). (A) Representative growth of WT and deletion strains *in planta* (*z*= 15 μm); Bar= 20 μm. (B) Magnification of the area boxed with white dashed lines in A, showing representative growth of the strains in more detail (*z*= 15 μm); Bar= 20 μm. (C) Representative hyphal branching and fusion of WT and deletion strains *in planta* (*z*= 5 μm); Bar= 10 μm.

Culture and *in planta* phenotype of overexpression strains

As the deletion of the four genes did not result in any obvious plant interaction phenotype, overexpression (OE) constructs were generated using the translation elongation factor (*tef*) promoter from *Aureobasidium pullulans*, which is commonly used for OE studies [37, 67]. Plasmids encoding the *gpiB*, *sspM*, *sspN* and *sspO* OE constructs (pBH29–32) were prepared and transformed into WT protoplasts and the copy number of 10 independent transformants for each construct determined (S4 Fig). A total of three strains per construct, each with a different copy number, were chosen for further analysis. In addition, the relative expression level of the gene in each of the three independent strains was determined and found to generally correlate with the copy number (S4 Fig). No difference in culture growth or morphology was observed between the OE strains and WT. To test the plant symbiotic phenotype, the OE strains were inoculated into *L. perenne* seedlings and infected plants examined 8 weeks post-planting. No difference in whole plant (Fig 10) or cellular phenotype (Fig 11) was observed between the OE strains and WT. In summary, these results demonstrate that overexpression of *gpiB*,

922 *sspM*, *sspN* or *sspO* has no impact on the culture or whole plant interaction
923 phenotype.
924
925 **Fig 10. Plant phenotype of *Lolium perenne* infected with *E. festucae* WT**
926 **and *gpiB, sspM, sspN* and *sspO* OE strains.** (A-D) Whole plant phenotype
927 of WT and OE strain-infected *L. perenne* plants 8 weeks post-planting. (E and
928 F) Boxplots representing tiller number (E) and length (F) of ryegrass plants eight
929 weeks post-planting with *E. festucae* WT (n= 2) and *gpiB* (n= 2/6/4), *sspM* (n=
930 3/2/6), *sspN* (n= 2/7/3) and *sspO* (n= 4/4) OE strains. One-way ANOVAs were
931 used to test for differences in both plant phenotypes between wildtype and
932 modified strains. In each case the ANOVA was fitted with R and a Bonferroni
933 correction was applied to all p-values to account for multiple testing.
934
935 **Fig 11. Confocal depth image series of *in planta* cellular phenotype of *E.***
936 ***festucae* WT and *gpiB, sspM, sspN and sspO* OE strains.** Infected *L.*
937 *perenne* pseudostem samples were stained with aniline blue/WGA-AF488.
938 Hyphae show aniline blue fluorescence of β-glucans (red pseudocolor) and
939 chitin staining of septa with WGA-AF488 (blue pseudocolor). (A)
940 Representative growth of WT and OE strains *in planta* (*z*= 15 µm); Bar= 20 µm.
941 (B) Magnification of the area boxed with white dashed lines in A, showing
942 representative growth of the strains in more detail (*z*= 15 nm); Bar= 20 µm. (C)
943 Hyphal branching and fusion of WT and OE strains *in planta* (*z*= 5 nm); Bar=
944 20 µm.
945

946 ## SspM, SspN and SspO localize extracellularly

947 To test whether SspM, SspN and SspO are translocated to the cytosol of the
948 host, we generated C-terminal mCherry fusion constructs of each protein under
949 the control of their native promoters. These constructs also contained three C-
950 terminal tandem repeats of the simian virus large T-antigen nuclear localization
951 signal to target the fusion proteins to the host nucleus, to enhance the signal in
952 the cell if the proteins are translocated to the plant cytosol [60]. The constructs
953 were transformed into protoplasts of their respective deletion strain, together
954 with a vector encoding cytoplasmic eGFP to facilitate identification of hyphae
955 among the plant cell background. Transformants were screened by PCR for
956 presence of the construct and then inoculated into *L. perenne* seedlings. Leaf
957 tissue was harvested from mature infected plants and examined by CSLM for
958 mCherry localization. Although the fluorescence from the mCherry fusion
959 proteins was generally weak *in planta*, a signal of sufficient intensity was
960 detected from SspM-mCherry-NLS and SspO-mCherry-NLS in the apoplast on
961 either side of the hyphae. For SspN-mCherry-NLS, the signal was so weak that
962 a localization profile for this protein in endophytic hyphae was not possible. No
963 evidence was found for localization of any of the three constructs to the plant
964 nucleus despite examining many individual sections and fields from different
965 plants inoculated with other transformants. By contrast, the signal for mCherry
966 in epiphyllous hyphae on the leaf surface was relatively strong and distinctly
967 localized along the cell walls for all three constructs, demonstrating that the
968 proteins were secreted *in planta,* but appear to remain attached to the hyphal
969 cell surface (Fig 12). These observations indicate that SspM, SspN and SspO
970 are secreted into the apoplast and may remain attached to the hyphal cell
971 surface post-secretion.

Fig 12. Confocal micrographs of the localization of SspM-mCherry-NLS, SspN-mCherry-NLS and SspO-mCherry-NLS in endophytic and epiphyllous hyphae of *E. festucae* in mature *L. perenne* plants. Besides the mCherry constructs each transformant contained eGFP to facilitate identification of the hyphae *in planta*; Bar= 10 µm.

SspM, SspN, SspO and GpiB do not elicit a defense response in *N. benthamiana* or *N. tabacum* and do not suppress INF1-triggered immunity in *N. benthamiana*

Several fungal effector proteins have been shown to activate the plant immune system (i.e. to trigger a cell death immune response) in non-host plants upon their recognition as 'invasion patterns' by corresponding plant immune receptor proteins [95]. To test whether non-host plants are able to recognize GpiB or the Ssps, as invasion patterns, each was expressed in *N. benthamiana* and *N. tabacum* leaf tissue using an *A. tumefaciens* transient expression assay and screened for an associated cell death response. For this purpose, the cDNA sequence encoding each mature protein (i.e. lacking a native secretion signal) was fused to the nucleotide sequence encoding the *N. tabacum* PR1α secretion signal (for secretion to the plant apoplast) and 3xFLAG (for detection by western blot), and ligated into the pICH86988 expression vector by Golden Gate cloning. The resulting expression vectors were then transformed into *A. tumefaciens* strain GV3101. Strains confirmed to contain the correct construct

were infiltrated into leaves of approx. five-week old *N. benthamiana* and *N. tabacum* plants, and the expression of GpiB and the three Ssps verified by western blotting using an antibody to the FLAG-Tag (S5 Fig). Plants were examined for any sign of a cell death response at one-week post-infiltration. As expected, the positive control, INF1 from *Phytophthora infestans* (a PAMP), triggered a strong cell death response in both *N. benthamiana* and *N. tabacum* (Figs 13A and B). As expected, the negative control, pICH86988 empty vector, failed to trigger cell death in these plants (Figs 13A and B). Unlike INF1, however, neither GpiB, nor the three Ssps, triggered cell death in *N. benthamiana* and *N. tabacum* (Figs 13A and B) suggesting that they are not recognized as invasion patterns by these non-host plants.

Many fungal effector proteins are anticipated to suppress activation of the plant immune response [1]. With this in mind, we next examined whether any of the four proteins are able to suppress the cell death response elicited by the INF1 PAMP in *N. benthamiana*, a model plant system for testing for this response. As before, responses were evaluated one-week post-infection. For this experiment, leaves were first infiltrated with the *A. tumefaciens* strain containing an expression vector for GpiB or one of the three Ssps. After 24 h, the same infiltration zone was infiltrated with the *A. tumefaciens* strain containing the INF1 expression vector. As the outcome of this experimental design is very sensitive to environmental influences, appropriate controls were included for each independent experiment. As expected, infiltration of an *A. tumefaciens* strain containing an expression vector for the *P. infestans* effector Avr3a 24 h after the corresponding potato resistance protein R3 resulted in a strong cell death response (Figs 13C and D). As expected, infiltration of an *A.*

tumefaciens strain containing an expression vector for eGFP 24 h before INF1, gave a strong cell death response, demonstrating that eGFP is not able to suppress the cell death response caused by INF1 (Figs 13C and D). When Avr3 was infiltrated 24 h before INF1, the PAMP-triggered cell death response normally elicited by INF1 was strongly suppressed (Figs 13C and D), confirming a previous study showing that Avr3a is able to suppress INF1-triggered cell death in *N. benthamiana* [96]. Unlike the results shown for Avr3a, infiltration of the three Ssps or GpiB, did not result in suppression of INF1-triggered cell death (Figs 13C and D).

Taken together, these experiments show that neither the Ssps, nor GpiB, are recognized by the non-host plants *N. tabacum* and *N. benthamiana*, and that these proteins are unable to suppress the cell death response triggered by INF1.

Fig 13. *A. tumefaciens* transient expression assays of GpiB, SspM, SspN and SspO in the non-host plants *N. benthamiana* and *N. tabacum*. (A) *N. benthamiana* and (B) *N. tabacum* leaf phenotypes in response to *A. tumefaciens* transient expression assays involving GpiB, SspM, SspN, SspO or INF1. INF1 triggers a strong cell death response, whereas the pICH86988 empty vector had no effect. (C and D) INF1-triggered cell death suppression assays in *N. benthamiana*. GpiB or any of the three Ssps were unable to suppress INF1-triggered cell death in *N. benthamiana*. eGFP was used as a negative control, INF1/Avr3a as a suppression control, and Avr3a/R3a as cell death positive control. All photos were taken one-week post-infiltration.

Discussion

Effectors of plant-pathogenic fungi function to promote host colonization, typically by suppressing the plant immune system. Current evidence, based on a small number of functionally characterized effectors from root endophytes [16-19], suggests that effectors from plant-mutualistic fungi play a similar role. In this study, we identified a suite of candidate effectors from the mutualistic symbiotic fungus *E. festucae*. We then performed an in-depth functional analysis in an attempt to uncover a role for three candidate effectors, representing some of the most highly expressed candidate effectors from this fungus *in planta*, in the mutualistic symbiotic interaction of *E. festucae* with *L. perenne*.

Making use of the completely annotated genome of *E. festucae* strain Fl1 and a combination of SignalP, EffectorP and protein size restriction we identified 141 genes encoding putative effectors. Eighty-three of these genes are homologous to uncharacterized proteins from other Sordariomycete genera, while a further nine have homologs in other *Epichloë* species. The repertoire of effectors present in the genome thus includes conserved proteins that may support somewhat generalized host-adaptation and a number of apparently lineage-specific genes. Effectors are known to contribute to host specificity in other plant-associated fungal species [97-99], and we predict some of the apparently lineage-specific effectors identified here will contribute to specific host interactions in *Epichloë* strains.

Having a complete and finished *E. festucae* genome sequence enabled us to test for association between structural features of the genome and genes encoding effectors. Our results are remarkable for the lack of associations that

1071 are well-documented in other fungal species. The *E. festucae* genome has a
1072 "patchwork" structure, in which distinct blocks of highly AT-biased DNA
1073 comprised almost entirely of TEs are interleaved with gene-rich regions that
1074 have balanced GC-content. This genome structure is similar to that found in the
1075 pathogenic fungus *L. maculans,* where effector genes are greatly over-
1076 represented within AT-rich blocks (comprising 80% of all genes in these
1077 regions). Similarly, it has been reported that effector-encoding genes are
1078 located in TE-rich regions of the *M. oryzae* [100], *Blumeria graminis* [101] and
1079 *F. oxysporum* [102] genomes [103]. In contrast, we found no evidence for
1080 enrichment of genes encoding candidate effectors in proximity to AT- and
1081 transposable element-rich regions. Indeed, only 5.7% of the candidate effector
1082 genes can be found within 1 kb of an AT-rich block and none were found within
1083 an AT-rich block.

1084 The lack of association between AT-rich blocks in the *E. festucae*
1085 genome and effectors is made more surprising by the evidence that these
1086 blocks contribute to plant-specific gene expression of other genes [26]. We
1087 have recently shown that the patchwork structure of the *E. festucae* genome
1088 strongly influences the resultant 3D conformation of the chromosomes, where
1089 AT-rich blocks mainly interact with other AT-rich blocks to generate a highly
1090 condensed chromatin state compared to the GC and gene-rich blocks. Genes
1091 specific to *E. festucae* as well as genes highly expressed during the interaction
1092 with the plant host were found to be overrepresented in proximity to the AT-rich
1093 blocks [26]. The fact effectors are not associated with the blocks, the rapidly
1094 evolving sub-telomeric regions, and do not form distinct clusters as found in
1095 other species, reflect the difference in evolutionary pressures experience by

symbiotic, rather than pathogenic, fungal species. However, we did find an enrichment of genes encoding secreted proteins in general and SSPs in particular, in proximity to MITEs. MITEs are small, non-autonomous DNA transposable elements abundantly distributed in eukaryotic genomes. Transposable elements are increasingly seen as important for gene regulation, and MITEs have been linked to gene expression traits in a number of species [27, 104]. In *E. festucae*, MITEs have been found in the promoter region of key secondary metabolite gene clusters [24, 105] and are greatly over-represented in the regions upstream of genes preferentially expressed *in planta* [26]. These results, and the demonstration here that genes encoding Ssps are frequently in close proximity to MITEs, suggests that elements either directly or indirectly associated with MITEs may play a key role in regulating the expression of *ssps*.

In the root endophyte *F. oxysporum,* most effector genes are encoded on a dispensable TE-rich pathogenicity chromosome [97, 106]. Recently a MITE from the mimp family was identified in the promoter region of each of the *SIX* effector genes and based on the presence of this mimp in the promoter region of other genes, further secreted proteins could be predicted and subsequently identified in the xylem sap of infected tomato plants [25]. Interestingly, deletion of the mimp element from the promoter region of two of the *SIX* genes did not significantly change the expression of these genes *in planta* or culture, thereby ruling out a direct role of this element in transcriptional regulation [25]. However, a putative transcriptional regulator (repressor) binding element in close proximity to the mimp is important for SIX gene expression. Whether the MITEs identified in *E. festucae* contribute to transcriptional silencing or activation remains to be elucidated.

Expression of effector genes is often induced upon plant infection or at a certain stage of host infection [87, 88]. Consistent with this observation we found a preferential expression of candidate effector-encoding genes *in planta.* Previous work has shown that a major remodeling of the *E. festucae* chromatin state occurs upon the switch from growth in axenic culture to growth *in planta*. In culture the genome is highly heterochromatic, characterized by high levels of H3K9me3 and H3K27me3, whereas *in planta* the genome contains higher levels of transcriptionally active euchromatin characterized by much lower levels of these two repressive epigenetic marks [68]. While RNAseq data for mutants of the responsible methyltransferases was not available, a set of data was available for a mutant of the gene encoding heterochromatin protein 1 (*hepA*). When a comparison was made between the transcriptome of Δ*hepA* vs WT in axenic culture there was a minor but significant increase in expression of the candidate effector genes. Similar results have been obtained in *L. maculans* where silencing of genes encoding the heterochromatin regulators DIM-5, a H3K9 methyl transferase, and heterochromatin protein 1 (HP1) resulted in the expression of many effector genes in axenic culture, which were repressed in WT [89]. As discussed above, effector genes in *L. maculans* are mainly located within the AT isochore component of the genome, which is in a highly heterochromatic state in axenic culture [89]. In contrast genes encoding *E. festucae* effectors are not associated with the AT-rich blocks of the genome and thus were expected to be less affected by heterochromatin silencing.

Previous studies have shown that the deletion of genes coding for NoxA, a NADPH oxidase [34], ProA, a transcription factor [39], and SakA, a stress-responsive MAP kinase [36], in *E. festucae* result in a severe breakdown in the

symbiotic interaction with the host leading to severely stunted plants. Analysis of the fungal transcriptome of these three different interactions identified a core set of 182 *E. festucae* genes that were differentially expressed (DE) in the same direction in all three symbiosis mutants [47]. Among this core gene set were 14 genes encoding secreted proteins, corresponding to 10 that were upregulated and four (*gpiB, sspM*, *sspN* and *sspO*), that were downregulated. The three putative effector genes analysed here were among the top 100 DE genes *in planta* compared to axenic culture.

In order to verify that the predicted secretion signals of the three effector candidates and the GPI-anchored protein were functional, a yeast complementation assay was carried out [52]. *S. cerevisiae* transformants containing each of the four predicted secretion signals fused to SUC2 all grew on raffinose confirming these signals are functional. In addition, western blots were performed with His-tagged versions of each of the four genes under the control of a *tef* promoter to confirm they were secreted and to check for proteolytic processing and any potential post-translational modifications. Both GpiB and SspM were predicted to be *N*-glycosylated and SspM and SspN contain a kexin cleavage site. Proteins of the expected size for GpiB, SspN and SspO were detected in extracts of fungal mycelia. For SspM, two signals were detected which potentially correspond to the pro-protein and a post-translationally modified protein. Some effectors, such as *C. fulvum* Avr4 and Avr9 are further processed in the apoplast by either fungal or plant proteases [20]. To determine whether there is protease modification of the SspM *in planta* and whether this processing is necessary for the activation of SspM will require further experimentation using protein extracts obtained from ryegrass

apoplastic fluid. Despite the presence of an LxKR kexin recognition motif in SspN, only a single band was detected corresponding to the size of the unprocessed protein. Sequence alignment with closely related species shows that this motif can only be found in strain FI1, suggesting this might be the result of a recent mutation. One possible reason for lack of cleavage at this site could be lack of accessibility of this motif within the folded protein. Alternatively, it is possible it is only cleaved *in planta* and not in axenic culture. While the function of SspN is not known it does have a repeat domain structure which is a common feature of several effectors characterized to date including Ecp6 from *C. fulvum* [107], which contains multiple LysM domain containing repeats, Sp7 from the mutualist *Glomus intraradices* [18], *Colletotrichium graminicola* EP1[108] and the recently identified effector Rsp3 from *U. maydis* [6]. However, unlike all these proteins, which have been shown by genetic analysis to be very important for the interaction with the host, deletion of *sspN* had no obvious plant interaction phenotype. Some of these repeat-containing effectors function in the apoplast (Ecp6 and Rsp3), whereas others are transported into the host cytoplasm (Sp7 and EP1). Due to the adoption of an extended module-like structure, some repeat-containing proteins such as EP1 are found to be associated with nucleic acids following transport into the host nucleus whereas others mediate protein-protein interactions [108-110]. In addition, some repeat-containing proteins are located on the surface of the cell where they are integrated into the plasma membrane or attached to the cell wall [109]. Rps3 is located on the *U. maydis* cell wall where it interacts with the mannose-binding and anti-fungal activity of the maize protein AFP1 [6]. Some repeat-containing proteins contain kexin cleavage sites between the repeating units resulting in

generation of bioactive peptides. A classic example of this in *Epichloë* is GigA, which is processed to generate a series of cyclic peptides called epichloëcyclins of unknown biological function [111]. In *U. maydis*, Rep1, is processed into smaller peptides that form cell wall associated fibrils mediating attachment of the hyphae to hydrophobic surfaces [112, 113].

Although products of all four genes could be detected in the fungal mycelium, only SspM and SspO, which contain six and eight cysteines respectively, were detected in the culture medium. The lack of detection of GpiB in the culture medium was not surprising as the addition of a GPI-anchor generally results in cell wall attachment. GPI-anchored proteins are involved in multiple processes, including attachment of hyphae to various surfaces, cell wall integrity and virulence [42, 43]. The two protein products observed for SspM in the media were the same size as those observed in the mycelia. The presence of two bands could either indicate that both the modified as well as the unmodified protein fulfill a function in *E. festucae* or that the overexpression of the gene because of multiple integrations resulted in an overproduction compared to the available protease. As the protein however can be detected in the modified version in culture and only one band can be detected in the western blot on SspM expressing *N. benthamiana* protein extracts, a modification by plant proteases to induce activity can probably be excluded. The inability to detect SspN in the culture media could be either due to the instability of the protein resulting from the lack of cysteines that promote stability or due to an attachment of this protein to the cell wall as has been described for multiple repeat-containing proteins as discussed above. A single protein product of the same size as observed in mycelia was detected in the media of

cultures containing the SspO construct indicating this protein is not post-translationally modified. The presence of eight cysteines, which have the potential to form four cysteine bridges, is likely to account for the high stability of this protein. Given the observed size for SspM was similar to the expected size, this proteins is probably not *N*-glycosylated. However the product of the His-tagged GpiB was greater than the predicted size, which may be due to addition of the GPI anchor and/or modification by *N*-glycosylation. For a definitive answer, purified proteins could be analyzed by mass spectrometry or subjected to an enzymatic removal of glycosylation followed by a size comparison using SDS-PAGE.

Some pathogens such as *U. maydis* produce apoplastic as well as cytoplasmic effectors [1], whereas other pathogens such as *C. fulvum* seem to only produce apoplastic effectors [72]. In order to determine where the effector candidates of *E. festucae* are targeted during host colonization, translational fusions were generated between each of the candidate genes and mCherry. Given it is difficult to detect effectors in the host cytoplasm, we used the method of adding a nuclear localization signal to target the proteins to the plant nucleus, as this was shown to be very effective for detecting some *M. oryzae* effectors in cells of the host *O. sativa* [60]. Despite examining multiple samples of different aged plants, no signal from any of the candidates was observed in the nuclei of ryegrass leaf cells. Therefore, the effector candidates are likely to reside in the apoplast. Indeed, we were able to show that all three of the effector candidates localized to the cell walls or plasma membrane of the fungal hyphae *in planta*. The clearest signals were obtained by imaging epiphyllous hyphae on the surface of the leaves. While it was more challenging to detect the

localization of these proteins inside the leaf, signals of sufficient intensity were detected for both SspM and SspO on the cell walls of endophytic hyphae. However, no signal could be detected for SspN in endophytic hyphae which could be due to the fact that the promoter of *sspN* is weaker than that of *sspM* and *sspO*. Alternatively, SspN may be more unstable in the apoplast than SspM and SspO as was suggested by the western analysis. Alternatively, *sspN* may be just expressed on the leaf surface. This hypothesis could be tested by fusing the promoter of *sspN* to eGFP and analyzing where fluorescence occurs.

To elucidate the role of these proteins in the interaction we generated deletion and overexpression strains and analysed their phenotype in axenic culture as well as in the interaction with perennial ryegrass. In culture, *E. festucae* forms white, soft looking colonies with a diameter of approx. 2 cm after 7 days of growth. Both deletion and overexpression strains were indistinguishable from the WT. Within the plant host, *E. festucae* grows exclusively in the apoplastic space, where the growth is highly regulated and synchronized with the host [114]. In the host meristematic tissue, *E. festucae* grows by tip growth, but as hyphal cells grow into the cell expansion zone of the leaf, the hyphae switch to intercalary growth, a pattern of growth that prevents mechanical shear and enables the hyphae to maintain the same rate of growth as the host [114, 115]. Ryegrass plants infected with either the deletion or overexpression strains had the same whole plant interaction and cellular growth phenotype as WT with one exception. Mutants Δ*gpiB*, Δ*sspM* and Δ*sspN* were seed transmitted but not Δ*sspO*. Additional long-term experiments will be necessary to determine the mechanism for this interesting Δ*sspO* phenotype. Also it would be interesting to check whether these mutants

affect the transition from asexual to sexual development but this is difficult to investigate as initiation of the sexual cycle requires vernalisation of host material, formation of stromata and transfer of spermatia to a stroma of the opposite mating type by a *Botanophila* fly [116]. Furthermore, it is possible that each of these effector candidates contributes to the interaction in a minor incremental way making it difficult to detect a phenotype by deletion of single effector gene unless there is a very sensitive phenotype screen [117, 118].

Functional redundancy of effector proteins could also explain the lack of an altered host interaction phenotype. Redundancy is thought to be the result of multiple effectors having the same or overlapping functions. Notably, a study by Weßling and colleagues [119] found effectors from a single pathogen species converging on interactions with a small subset of host proteins in a process named “interspecies convergence” of which many are involved in high level regulatory processes. Interestingly, even effectors from different species of pathogens can target a similar subset of host proteins with a correlation between the degree of convergence and the relevance of the host protein. Therefore homology-independent functional redundancy is maintained as an evolutionary benefit and protects against rapid loss of a single effector due to host recognition [119, 120]. For example, both Avr4 and Ecp6 prevent chitin recognition in the *C. fulvum*-tomato interaction, however, the molecular functions are different and there is no sequence homology between these two effectors [2, 4].

In the presence of a corresponding host immune receptor protein, fungal effectors are known to activate the plant immune system. Often, the main output of this activation is the hypersensitive response (HR), which renders the host

resistant and the pathogen avirulent [121]. Notably, a subset of fungal effectors can also trigger an HR-like cell death response when expressed in the non-host plants *N. benthamiana* or *N. tabacum* (i.e. following their recognition by unknown immune receptor proteins) using an *A. tumefaciens* transient expression assay. Indeed, multiple effectors of the wheat pathogen *Z. tritici* have been found to induce an HR in *N. benthamiana* [95]. Using this approach, we tested whether the three candidate effectors of *E. festucae* trigger cell death when produced by these two non-host plants but none triggered a cell death response. We also tested whether the effector candidates are able to suppress a defense response triggered by the *P. infestans* elicitor INF1 using an *A. tumefaciens* transient expression assay. INF1 functions in the apoplastic space where it binds to the ELR (elicitin response) receptor, resulting in activation of the plant immune system [122, 123]. Even though these candidate effectors localize to the apoplast, none were able to suppress INF1-triggered immunity.

In *E. festucae*-infected *L. perenne* plants, approx. one third of *L. perenne* genes were found to be differentially expressed compared to non-infected plants. These changes were found to be in the key areas of ‘stress response’, ‘primary metabolism’ and ‘secondary metabolism’ [124]. Genes in the category ‘primary metabolism’ and ‘stress response’, including PR genes, were found to be mainly downregulated, and genes involved in secondary metabolism were found to be upregulated [124]. These findings, together with the fact that these candidate effectors are so highly expressed in *E. festucae in planta*, suggests that these proteins are likely to have a key role in the interaction. Furthermore, microscopic studies in infected *L. perenne* plants revealed a lack of chitin, a crucial PAMP, in endophytic hyphae [124, 125]. This indicates that chitin is

either masked, potentially by a similar mechanism as has been described for Avr4 of *C. fulvum,* or modified.

In this study, we have identified for the first time, a suite of effector candidates from the grass endophyte *E. festucae*. Genes encoding effector candidates were found to associate with MITEs but not with AT-rich regions or TEs, indicating that they might not be under strong selection pressure. Three effector candidates were functionally analysed but were found to be dispensable for the interaction with *L. perenne* under the growth conditions analysed. Although we could not find any evidence for a role for any of these effectors in the interaction, the list of effector candidates identified provides a good database for selecting other proteins and strategies for functional analysis. Sequencing of additional *Epichloë* species will help identify effector genes conserved across species or unique to one species and thereby provide important insights into the role of these effectors in host specificity in this agriculturally important symbiosis.

Acknowledgements

This research was supported by grants from the Tertiary Education Commission to the Bio-Protection Research Centre, the Royal Society of New Zealand Marsden Fund (contract MAU1301) and by Massey University. The authors thank Jordan Taylor, Niki Murray and Matthew Savoian (Manawatu Microscopy and Imaging Centre, Massey University) for assistance with microscopy, Arvina Ram and Karolin Warnecke for technical assistance, Christopher Schardl for provision of the *Epichloë* database sequences, Melissa Guo for provision of strains and advice on *Agrobacterium* infiltration assays, and Sophian Kamoun and Barbara Valent for provision of plasmids.

Author contributions

Conceptualization: BH DW CHM CJE BS.

Data curation: BH DW.

Formal analysis: BH DW CHM.

Funding acquisition: BS.

Investigation: BS DW.

Methodology: BH DW YB CHM CJE BS.

Project Administration: BS.

Resources: BS.

Supervision: CHM CJE BS.

Writing – original draft: BH DW CHM BS.

Writing – review & editing: CHM CJE BS.

References

1. Lo Presti L, Lanver D, Schweizer G, Tanaka S, Liang L, Tollot M, et al. Fungal effectors and plant susceptibility. Annu Rev Plant Biol. 2015;66:513-45. doi: 10.1146/annurev-arplant-043014-114623. PubMed PMID: 25923844.

2. van den Burg HA, Harrison SJ, Joosten MH, Vervoort J, de Wit PJ. *Cladosporium fulvum* Avr4 protects fungal cell walls against hydrolysis by plant chitinases accumulating during infection. Mol Plant-Microbe Interact. 2006;19(12):1420-30. PubMed PMID: 17153926.

3. van Esse HP, Van't Klooster JW, Bolton MD, Yadeta KA, van Baarlen P, Boeren S, et al. The *Cladosporium fulvum* virulence protein Avr2 inhibits host proteases required for basal defense. Plant Cell. 2008;20(7):1948-63. Epub 2008/07/29. doi: 10.1105/tpc.108.059394. PubMed PMID: 18660430; PubMed Central PMCID: PMCPMC2518240.

4. de Jonge R, van Esse HP, Kombrink A, Shinya T, Desaki Y, Bours R, et al. Conserved fungal LysM effector Ecp6 prevents chitin-triggered immunity in plants. Science. 2010;329(5994):953-35. Epub 2010/08/21. doi: 329/5994/953 [pii]
10.1126/science.1190859. PubMed PMID: 20724636.

5. Doehlemann G, Reissmann S, Assmann D, Fleckenstein M, Kahmann R. Two linked genes encoding a secreted effector and a membrane protein are essential for *Ustilago maydis*-induced tumour formation. Mol Microbiol. 2011;81(3):751-66. doi: 10.1111/j.1365-2958.2011.07728.x. PubMed PMID: 21692877.

1386 6. Ma LS, Wang L, Trippel C, Mendoza-Mendoza A, Ullmann S, Moretti
1387 M, et al. The *Ustilago maydis* repetitive effector Rsp3 blocks the antifungal
1388 activity of mannose-binding maize proteins. Nature communications.
1389 2018;9(1):1711. doi: 10.1038/s41467-018-04149-0. PubMed PMID:
1390 29703884; PubMed Central PMCID: PMC5923269.
1391 7. Hurlburt NK, Chen L-H, Stergiopoulos I, Fisher AJ. Structure of the
1392 *Cladosporium fulvum* Avr4 effector in complex with (GlcNAc)6 reveals the
1393 ligand-binding mechanism and uncouples its intrinsic function from recognition
1394 by the Cf-4 resistance protein. PLoS Pathog. 2018;14(8):e1007263. Epub
1395 2018/08/28. doi: 10.1371/journal.ppat.1007263. PubMed PMID: 30148881;
1396 PubMed Central PMCID: PMCPMC6128652.
1397 8. Sánchez-Vallet A, Saleem-Batcha R, Kombrink A, Hansen G,
1398 Valkenburg D-J, Thomma BPHJ, et al. Fungal effector Ecp6 outcompetes
1399 host immune receptor for chitin binding through intrachain LysM dimerization.
1400 Elife. 2013;2:e00790. Epub 2013/07/11. doi: 10.7554/eLife.00790. PubMed
1401 PMID: 23840930; PubMed Central PMCID: PMCPMC3700227.
1402 9. Mueller AN, Ziemann S, Treitschke S, Assmann D, Doehlemann G.
1403 Compatibility in the *Ustilago maydis*-maize interaction requires inhibition of
1404 host cysteine proteases by the fungal effector Pit2. PLoS Pathog.
1405 2013;9(2):e1003177. doi: 10.1371/journal.ppat.1003177. PubMed PMID:
1406 23459172; PubMed Central PMCID: PMC3573112.
1407 10. Rooney HCE, Van't Klooster JW, van der Hoorn RAL, Joosten MHAJ,
1408 Jones JDG, de Wit PJGM. Cladosporium Avr2 inhibits tomato Rcr3 protease
1409 required for *Cf-2*-dependent disease resistance. Science.

2005;308(5729):1783-6. Epub 2005/04/23. doi: 10.1126/science.1111404. PubMed PMID: 15845874.

11. Shabab M, Shindo T, Gu C, Kaschani F, Pansuriya T, Chintha R, et al. Fungal effector protein AVR2 targets diversifying defense-related cys proteases of tomato. Plant Cell. 2008;20(4):1169-83. Epub 2008/05/03. doi: 10.1105/tpc.107.056325. PubMed PMID: 18451324; PubMed Central PMCID: PMCPMC2390736.

12. Djamei A, Schipper K, Rabe F, Ghosh A, Vincon V, Kahnt J, et al. Metabolic priming by a secreted fungal effector. Nature. 2011;478(7369):395-8. Epub 2011/10/07. doi: nature10454 [pii] 10.1038/nature10454. PubMed PMID: 21976020.

13. O'Connell RJ, Panstruga R. Tête à tête inside a plant cell: establishing compatibility between plants and biotrophic fungi and oomycetes. New Phytol. 2006;171(4):699-718. Epub 2006/08/22. doi: 10.1111/j.1469-8137.2006.01829.x. PubMed PMID: 16918543.

14. Zamioudis C, Pieterse CMJ. Modulation of host immunity by beneficial microbes. Mol Plant-Microbe Interact. 2012;25(2):139-50. Epub 2011/10/15. doi: 10.1094/MPMI-06-11-0179. PubMed PMID: 21995763.

15. Pauwels L, Goossens A. The JAZ proteins: a crucial interface in the jasmonate signaling cascade. Plant Cell. 2011;23(9):3089-100. Epub 2011/10/04. doi: 10.1105/tpc.111.089300. PubMed PMID: 21963667; PubMed Central PMCID: PMCPMC3203442.

16. Plett JM, Kemppainen M, Kale SD, Kohler A, Legue V, Brun A, et al. A secreted effector protein of *Laccaria bicolor* is required for symbiosis

1434 development. Curr Biol. 2011;21(14):1197-203. doi:
1435 10.1016/j.cub.2011.05.033. PubMed PMID: 21757352.
1436 17. Plett JM, Daguerre Y, Wittulsky S, Vayssieres A, Deveau A, Melton SJ,
1437 et al. Effector MiSSP7 of the mutualistic fungus *Laccaria bicolor* stabilizes the
1438 Populus JAZ6 protein and represses jasmonic acid (JA) responsive genes.
1439 Proc Natl Acad Sci USA. 2014;111(22):8299-304. doi:
1440 10.1073/pnas.1322671111. PubMed PMID: 24847068; PubMed Central
1441 PMCID: PMC4050555.
1442 18. Kloppholz S, Kuhn H, Requena N. A secreted fungal effector of
1443 *Glomus intraradices* promotes symbiotic biotrophy. Curr Biol.
1444 2011;21(14):1204-9. doi: 10.1016/j.cub.2011.06.044. PubMed PMID:
1445 21757354.
1446 19. Wawra S, Fesel P, Widmer H, Timm M, Seibel J, Leson L, et al. The
1447 fungal-specific beta-glucan-binding lectin FGB1 alters cell-wall composition
1448 and suppresses glucan-triggered immunity in plants. Nature communications.
1449 2016;7:13188. doi: 10.1038/ncomms13188. PubMed PMID: 27786272.
1450 20. Stergiopoulos I, de Wit PJGM. Fungal effector proteins. Annu Rev
1451 Phytopathol. 2009;47:233-63. Epub 2009/04/30. doi:
1452 10.1146/annurev.phyto.112408.132637. PubMed PMID: 19400631.
1453 21. Rouxel T, Grandaubert J, Hane JK, Hoede C, van de Wouw AP,
1454 Couloux A, et al. Effector diversification within compartments of the
1455 *Leptosphaeria maculans* genome affected by Repeat-Induced Point
1456 mutations. Nature communications. 2011;2:202. doi: 10.1038/ncomms1189.
1457 PubMed PMID: 21326234; PubMed Central PMCID: PMC3105345.

1458 22. Raffaele S, Kamoun S. Genome evolution in filamentous plant
1459 pathogens: why bigger can be better. Nat Rev Microbiol. 2012;10(6):417-30.
1460 Epub 2012/05/09. doi: 10.1038/nrmicro2790. PubMed PMID: 22565130.
1461 23. Feschotte C, Mouches C. Evidence that a family of miniature inverted-
1462 repeat transposable elements (MITEs) from the *Arabidopsis thaliana* genome
1463 has arisen from a pogo-like DNA transposon. Mol Biol Evol. 2000;17(5):730-7.
1464 Epub 2000/04/26. doi: 10.1093/oxfordjournals.molbev.a026351. PubMed
1465 PMID: 10779533.
1466 24. Fleetwood DJ, Khan AK, Johnson RD, Young CA, Mittal S, Wrenn RE,
1467 et al. Abundant degenerate miniature inverted-repeat transposable elements
1468 in genomes of epichloid fungal endophytes of grasses. Genome Biol Evol.
1469 2011;3:1253-64. Epub 2011/09/29. doi: evr098 [pii]
1470 10.1093/gbe/evr098. PubMed PMID: 21948396; PubMed Central PMCID:
1471 PMC3227409.
1472 25. Schmidt SM, Houterman PM, Schreiver I, Ma L, Amyotte S, Chellappan
1473 B, et al. MITEs in the promoters of effector genes allow prediction of novel
1474 virulence genes in *Fusarium oxysporum*. BMC Genomics. 2013;14:119. doi:
1475 10.1186/1471-2164-14-119. PubMed PMID: 23432788; PubMed Central
1476 PMCID: PMC3599309.
1477 26. Winter DJ, Ganley ARD, Young CA, Liachko I, Schardl CL, Dupont PY,
1478 et al. Repeat elements organise 3D genome structure and mediate
1479 transcription in the filamentous fungus *Epichloë festucae*. PLoS Genet.
1480 2018;14(10):e1007467. Epub 2018/10/26. doi:
1481 10.1371/journal.pgen.1007467. PubMed PMID: 30356280.

1482 27. Fattash I, Rooke R, Wong A, Hui C, Luu T, Bhardwaj P, et al. Miniature
1483 inverted-repeat transposable elements: discovery, distribution, and activity.
1484 Genome. 2013;56(9):475-86. Epub 2013/10/31. doi: 10.1139/gen-2012-0174.
1485 PubMed PMID: 24168668.
1486 28. Schardl CL, Scott B, Florea S, Zhang D. Epichloe endophytes:
1487 clavicipitaceous symbionts of grasses. In: Deising HB, editor. The Mycota
1488 Volume V - Plant Relationships. Berlin: Springer-Verlag; 2009. p. 275-306.
1489 29. Leuchtmann A, Schardl CL, Siegel MR. Sexual compatibility and
1490 taxonomy of a new species of *Epichloë* symbiotic with fine fescue grasses.
1491 Mycologia. 1994;86:802-12.
1492 30. Schardl CL, Leuchtmann A, Tsai H-F, Collett MA, Watt DM, Scott DB.
1493 Origin of a fungal symbiont of perennial ryegrass by interspecific hybridization
1494 of a mutualist with the ryegrass choke pathogen, *Epichloë typhina*. Genetics.
1495 1994;136:1307-17.
1496 31. Chung K-R, Schardl CL. Sexual cycle and horizontal transmission of
1497 the grass symbiont, *Epichloë typina*. Mycol Res. 1997;101(3):295-301.
1498 32. Scott B, Schardl C. Fungal symbionts of grasses: evolutionary insights
1499 and agricultural potential. Trends Microbiol. 1993;1(5):196-200.
1500 33. Chung K-R, Hollin W, Siegel MR, Schardl CL. Genetics of host
1501 specifictiy in *Epichloë typhina*. Phytopathology. 1997;87(6):599-605.
1502 34. Tanaka A, Christensen MJ, Takemoto D, Park P, Scott B. Reactive
1503 oxygen species play a role in regulating a fungus-perennial ryegrass
1504 mutualistic association. Plant Cell. 2006;18:1052-66.
1505 35. Takemoto D, Kamakura S, Saikia S, Becker Y, Wrenn R, Tanaka A, et
1506 al. Polarity proteins Bem1 and Cdc24 are components of the filamentous

1507 fungal NADPH oxidase complex. Proc Natl Acad Sci USA. 2011;108(7):2861-
1508 6.
1509 36. Eaton CJ, Cox MP, Ambrose B, Becker M, Hesse U, Schardl CL, et al.
1510 Disruption of signaling in a fungal-grass symbiosis leads to pathogenesis.
1511 Plant Physiol. 2010;153(4):1780-94. Epub 2010/06/04. doi: pp.110.158451
1512 [pii]
1513 10.1104/pp.110.158451. PubMed PMID: 20519633.
1514 37. Takemoto D, Tanaka A, Scott B. A p67(Phox)-like regulator is recruited
1515 to control hyphal branching in a fungal-grass mutualistic symbiosis. Plant Cell.
1516 2006;18(10):2807-21. PubMed PMID: 17041146.
1517 38. Tanaka A, Takemoto D, Hyon GS, Park P, Scott B. NoxA activation by
1518 the small GTPase RacA is required to maintain a mutualistic symbiotic
1519 association between *Epichloë festucae* and perennial ryegrass. Mol Microbiol.
1520 2008;68(5):1165-78. PubMed PMID: 18399936.
1521 39. Tanaka A, Cartwright GM, Saikia S, Kayano Y, Takemoto D, Kato M, et
1522 al. ProA, a transcriptional regulator of fungal fruiting body development,
1523 regulates leaf hyphal network development in the *Epichloë festucae-Lolium*
1524 *perenne* symbiosis. Mol Microbiol. 2013;90(3):551-68. doi: doi:
1525 10.1111/mmi.12385.
1526 40. Becker Y, Eaton CJ, Brasell E, May KJ, Becker M, Hassing B, et al.
1527 The fungal cell wall integrity MAPK cascade is crucial for hyphal network
1528 formation and maintenance of restrictive growth of *Epichloë festucae* in
1529 symbiosis with *Lolium perenne*. Mol Plant-Microbe Interact. 2015;28:69-85.
1530 doi: doi:10.1094/MPMI-06-14-0183-R.

1531 41. Sperschneider J, Gardiner DM, Dodds PN, Tini F, Covarelli L, Singh
1532 KB, et al. EffectorP: predicting fungal effector proteins from secretomes using
1533 machine learning. New Phytol. 2016;210(2):743-61. doi: 10.1111/nph.13794.
1534 PubMed PMID: 26680733.
1535 42. Rittenour WR, Harris SD. Glycosylphosphatidylinositol-anchored
1536 proteins in *Fusarium graminearum*: inventory, variability, and virulence. PLoS
1537 One. 2013;8(11):e81603. doi: 10.1371/journal.pone.0081603. PubMed PMID:
1538 24312325; PubMed Central PMCID: PMC3843709.
1539 43. Zhu W, Wei W, Wu Y, Zhou Y, Peng F, Zhang S, et al. BcCFEM1, a
1540 CFEM domain-containing protein with putative GPI-anchored site, is involved
1541 in pathogenicity, conidial production, and stress tolerance in *Botrytis cinerea*.
1542 Frontiers in microbiology. 2017;8:1807. Epub 2017/10/06. doi:
1543 10.3389/fmicb.2017.01807. PubMed PMID: 28979251; PubMed Central
1544 PMCID: PMC5611420.
1545 44. Petersen TN, Brunak S, von Heijne G, Nielsen H. SignalP 4.0:
1546 discriminating signal peptides from transmembrane regions. Nat Methods.
1547 2011;8(10):785-6. Epub 2011/10/01. doi: nmeth.1701 [pii]
1548 10.1038/nmeth.1701. PubMed PMID: 21959131.
1549 45. R development core team. R: A language and environment for
1550 statistical computing. R Foundation for Statistical Computing, Vienna, Austria.
1551 2013;URL https://www.R-project.org/.
1552 46. Quinlan AR. BEDTools: The swiss-army tool for genome feature
1553 analysis. Curr Protoc Bioinformatics. 2014;47:11.2. 1-34. Epub 2014/09/10.
1554 doi: 10.1002/0471250953.bi1112s47. PubMed PMID: 25199790; PubMed
1555 Central PMCID: PMCPMC4213956.

1556 47. Eaton CJ, Dupont P-Y, Solomon PS, Clayton W, Scott B, Cox MP. A
1557 core gene set describes the molecular basis of mutualism and antagonism in
1558 *Epichloë* species. Mol Plant-Microbe Interact. 2015;28:218-31. doi:
1559 doi.org/10.1094/MPMI-09-14-0293-FI.
1560 48. Lachner M, O'Carroll D, Rea S, Mechtler K, Jenuwein T. Methylation of
1561 histone H3 lysine 9 creates a binding site for HP1 proteins. Nature.
1562 2001;410(6824):116-20. doi: 10.1038/35065132. PubMed PMID: 11242053.
1563 49. Maison C, Almouzni G. HP1 and the dynamics of heterochromatin
1564 maintenance. Nat Rev Mol Cell Biol. 2004;5(4):296-304. doi:
1565 10.1038/nrm1355. PubMed PMID: 15071554.
1566 50. Miller JH. Experiments in Molecular Genetics. New York: Cold Spring
1567 Harbor Laboratory Press; 1972.
1568 51. Sambrook J, Fritsch EF, Maniatis T. Molecular cloning: a laboratory
1569 manual. Cold Spring Harbor, New York: Cold Spring Harbor Laboratory Press;
1570 1989.
1571 52. Jacobs KA, Collins-Racie LA, Colbert M, Duckett M, Golden-Fleet M,
1572 Kelleher K, et al. A genetic selection for isolating cDNAs encoding secreted
1573 proteins. Gene. 1997;198(1-2):289-96. PubMed PMID: 9370294.
1574 53. Ausubel FM, Brent R, Kingston RE, Moore DD, Seidman JG, Smith JA,
1575 et al. Current Protocols in Molecular Biology. New York.: John Wiley & Sons;
1576 1993.
1577 54. Moon CD, Tapper BA, Scott B. Identification of *Epichloë* endophytes *in*
1578 *planta* by a microsatellite-based PCR fingerprinting assay with automated
1579 analysis. Appl Environ Microbiol. 1999;65:1268-79.

1580 55. Moon CD, Scott B, Schardl CL, Christensen MJ. The evolutionary
1581 origins of *Epichloë* endophytes from annual ryegrasses. Mycologia.
1582 2000;92:1103-18.
1583 56. Latch GCM, Christensen MJ. Artificial infection of grasses with
1584 endophytes. Ann Appl Biol. 1985;107(1):17-24.
1585 57. Byrd AD, Schardl CL, Songlin PJ, Mogen KL, Siegel MR. The β-tubulin
1586 gene of *Epichloë typhina* from perennial ryegrass (*Lolium perenne*). Curr
1587 Genet. 1990;18(4):347-54.
1588 58. Gibson DG, Young L, Chuang RY, Venter JC, Hutchison CA, III, Smith
1589 HO. Enzymatic assembly of DNA molecules up to several hundred kilobases.
1590 Nat Methods. 2009;6(5):343-5. Epub 2009/04/14. doi: nmeth.1318 [pii]
1591 10.1038/nmeth.1318. PubMed PMID: 19363495.
1592 59. Eisenhaber B, Schneider G, Wildpaner M, Eisenhaber F. A sensitive
1593 predictor for potential GPI lipid modification sites in fungal protein sequences
1594 and its application to genome-wide studies for *Aspergillus nidulans*, *Candida*
1595 *albicans*, *Neurospora crassa*, *Saccharomyces cerevisiae* and
1596 *Schizosaccharomyces pombe*. J Mol Biol. 2004;337(2):243-53. doi:
1597 10.1016/j.jmb.2004.01.025. PubMed PMID: 15003443.
1598 60. Khang CH, Berruyer R, Giraldo MC, Kankanala P, Park SY, Czymmek
1599 K, et al. Translocation of *Magnaporthe oryzae* effectors into rice cells and their
1600 subsequent cell-to-cell movement. Plant Cell. 2010;22(4):1388-403. Epub
1601 2010/05/04. doi: tpc.109.069666 [pii]
1602 10.1105/tpc.109.069666. PubMed PMID: 20435900; PubMed Central PMCID:
1603 PMC2879738.

1604 61. Winston F, Dollard C, Ricupero-Hovasse SL. Construction of a set of
1605 convenient *Saccharomyces cerevisiae* strains that are isogenic to S288C.
1606 Yeast. 1995;11(1):53-5. Epub 1995/01/01. doi: 10.1002/yea.320110107.
1607 PubMed PMID: 7762301.
1608 62. Gietz RD, Woods RA. Transformation of yeast by lithium
1609 acetate/single-stranded carrier DNA/polyethylene glycol method. Meth
1610 Enzymol. 2002;350:87-96. Epub 2002/06/21. PubMed PMID: 12073338.
1611 63. Koncz C, Martini N, Szabados L, Hrouda M, Bachmair A, Schell J.
1612 Specialized vectors for gene tagging and expression studies. In: Gelvin SB,
1613 Schilperoort RA, editors. Plant Molecular Biology Manual. Dordrecht: Kluwer
1614 Academic; 1994. p. 1-22.
1615 64. Weigel D, Glazebrook J. Transformation of Agrobacterium using the
1616 freeze-thaw method. CSH Protoc. 2006;pdb.prot4666.
1617 65. Young CA, Bryant MK, Christensen MJ, Tapper BA, Bryan GT, Scott B.
1618 Molecular cloning and genetic analysis of a symbiosis-expressed gene cluster
1619 for lolitrem biosynthesis from a mutualistic endophyte of perennial ryegrass.
1620 Mol Gen Genomics. 2005;274:13-29.
1621 66. Itoh Y, Johnson R, Scott B. Integrative transformation of the mycotoxin-
1622 producing fungus, *Penicillium paxilli*. Curr Genet. 1994;25:508-13.
1623 67. Lukito Y, Chujo T, Scott B. Molecular and cellular analysis of the pH
1624 response transcription factor PacC in the fungal symbiont *Epichloë festucae*.
1625 Fungal Genet Biol. 2015;85:25-37. doi: 10.1016/j.fgb.2015.10.008. PubMed
1626 PMID: 26529380.
1627 68. Chujo T, Scott B. Histone H3K9 and H3K27 methylation regulates
1628 fungal alkaloid biosynthesis in a fungal endophyte-plant symbiosis. Mol

1629 Microbiol. 2014;92(2):413-34. Epub 2014/02/28. doi: 10.1111/mmi.12567.
1630 PubMed PMID: 24571357.
1631 69. Becker Y, Green K, Scott B, Becker M. Artificial inoculation of *Epichloë*
1632 *festucae* into *Lolium perenne*, and visualization of endophytic and epiphyllous
1633 fungal growth. Bio-protocol 2018;8:e2990.
1634 70. Florea S, Schardl CL, Hollin W. Detection and isolation of *Epichloë*
1635 species, fungal endophytes of grasses. Current protocols in microbiology.
1636 2015;38:19A.1.-A.1.24. Epub 2015/08/04. doi:
1637 10.1002/9780471729259.mc19a01s38. PubMed PMID: 26237108.
1638 71. Spiers AG, Hopcroft DH. Black canker and leaf spot of Salix in New
1639 Zealand caused by *Glomerella miyabeana* (*Colletotrichum gloeosporioides*).
1640 Eur J Forest Pathol. 1993;23:92-102.
1641 72. Mesarich CH, Ökmen B, Rovenich H, Griffiths SA, Wang C, Karimi
1642 Jashni M, et al. Specific hypersensitive response-associated recognition of
1643 new apoplastic effectors from *Cladosporium fulvum* in wild tomato. Mol Plant-
1644 Microbe Interact. 2018;31(1):145-62. doi: 10.1094/MPMI-05-17-0114-FI.
1645 PubMed PMID: 29144204.
1646 73. Joosten MHAJ, Vogelsang R, Cozijnsen TJ, Verberne MC, de Wit
1647 PJGM. The biotrophic fungus *Cladosporium fulvum* circumvents *Cf-4*-
1648 mediated resistance by producing unstable AVR4 elicitors. Plant Cell.
1649 1997;9(3):367-79.
1650 74. Luderer R, De Kock MJD, Dees RHL, De Wit PJGM, Joosten MHAJ.
1651 Functional analysis of cysteine residues of ECP elicitor proteins of the fungal
1652 tomato pathogen *Cladosporium fulvum*. Mol Plant Pathol. 2002;3(2):91-5.

1653 Epub 2002/03/01. doi: 10.1046/j.1464-6722.2001.00095.x. PubMed PMID:
1654 20569313.
1655 75. Kämper J, Kahmann R, Bolker M, Ma LJ, Brefort T, Saville BJ, et al.
1656 Insights from the genome of the biotrophic fungal plant pathogen *Ustilago*
1657 *maydis*. Nature. 2006;444(7115):97-101. doi: 10.1038/nature05248. PubMed
1658 PMID: 17080091.
1659 76. Brefort T, Tanaka S, Neidig N, Doehlemann G, Vincon V, Kahmann R.
1660 Characterization of the largest effector gene cluster of *Ustilago maydis*. PLoS
1661 Pathog. 2014;10(7):e1003866. doi: 10.1371/journal.ppat.1003866. PubMed
1662 PMID: 24992561; PubMed Central PMCID: PMC4081774.
1663 77. Cambareri EB, Jensen BC, Schabtach E, Selker EU. Repeat-induced
1664 G-C to A-T mutations in *Neurospora*. Science. 1989;244(4912):1571-5.
1665 PubMed PMID: 2544994.
1666 78. Gladyshev E. Repeat-induced point mutation and other genome
1667 defense mechanisms in fungi. Microbiol Spectrum. 2017;5(4):FUNK-0042-
1668 2017. doi: 10.1128/microbiolspec.FUNK-0042-2017. PubMed PMID:
1669 28721856; PubMed Central PMCID: PMC5607778.
1670 79. Cambareri EB, Singer MJ, Selker EU. Recurrence of repeat-induced
1671 point mutation (RIP) in *Neurospora crassa*. Genetics. 1991;127(4):699-710.
1672 Epub 1991/04/01. PubMed PMID: 1827629; PubMed Central PMCID:
1673 PMCPMC1204397.
1674 80. Fudal I, Ross S, Brun H, Besnard AL, Ermel M, Kuhn ML, et al.
1675 Repeat-induced point mutation (RIP) as an alternative mechanism of
1676 evolution toward virulence in Leptosphaeria maculans. Mol Plant-Microbe

1677 Interact. 2009;22(8):932-41. Epub 2009/07/11. doi: 10.1094/MPMI-22-8-0932.
1678 PubMed PMID: 19589069.
1679 81. Wong S, Wolfe KH. Birth of a metabolic gene cluster in yeast by
1680 adaptive gene relocation. Nature Genetics. 2005;37(7):777-82. PubMed
1681 PMID: 15951822.
1682 82. Orbach MJ, Farrall L, Sweigard JA, Chumley FG, Valent B. A telomeric
1683 avirulence gene determines efficacy for the rice blast resistance gene *Pi-ta*.
1684 Plant Cell. 2000;12(11):2019-32.
1685 83. Rehmeyer C, Li W, Kusaba M, Kim YS, Brown D, Staben C, et al.
1686 Organization of chromosome ends in the rice blast fungus, *Magnaporthe*
1687 *oryzae*. Nucleic Acids Res. 2006;34(17):4685-701. PubMed PMID: 16963777.
1688 84. Brown CA, Murray AW, Verstrepen KJ. Rapid expansion and functional
1689 divergence of subtelomeric gene families in yeasts. Curr Biol.
1690 2010;20(10):895-903. Epub 2010/05/18. doi: 10.1016/j.cub.2010.04.027.
1691 PubMed PMID: 20471265; PubMed Central PMCID: PMC2877759.
1692 85. Hirsch CD, Springer NM. Transposable element influences on gene
1693 expression in plants. Biochim Biophys Acta Gene Regul Mech.
1694 2017;1860(1):157-65. Epub 2016/05/29. doi: 10.1016/j.bbagrm.2016.05.010.
1695 PubMed PMID: 27235540.
1696 86. Chuong EB, Elde NC, Feschotte C. Regulatory activities of
1697 transposable elements: from conflicts to benefits. Nat Rev Genet.
1698 2016;18(2):71-86. doi: 10.1038/nrg.2016.139. PubMed PMID: 27867194.
1699 87. Lanver D, Müller AN, Happel P, Schweizer G, Haas FB, Franitza M, et
1700 al. The biotrophic development of *Ustilago maydis* studied by RNA-Seq

1701 analysis. Plant Cell. 2018;30(2):300-23. doi: 10.1105/tpc.17.00764. PubMed
1702 PMID: 29371439; PubMed Central PMCID: PMC5868686.
1703 88. Kleemann J, Rincon-Rivera LJ, Takahara H, Neumann U, Ver Loren
1704 van Themaat E, van der Does HC, et al. Sequential delivery of host-induced
1705 virulence effectors by appressoria and intracellular hyphae of the
1706 phytopathogen *Colletotrichum higginsianum*. PLoS Pathog.
1707 2012;8(4):e1002643. Epub 2012/04/13. doi: 10.1371/journal.ppat.1002643.
1708 PubMed PMID: 22496661; PubMed Central PMCID: PMCPMC3320591.
1709 89. Soyer JL, El Ghalid M, Glaser N, Ollivier B, Linglin J, Grandaubert J, et
1710 al. Epigenetic control of effector gene expression in the plant pathogenic
1711 fungus *Leptosphaeria maculans*. PLoS Genet. 2013;10(3):e1004227. Epub
1712 2014/03/08. doi: 10.1371/journal.pgen.1004227
1713 PGENETICS-D-13-03255 [pii]. PubMed PMID: 24603691; PubMed Central
1714 PMCID: PMC3945186.
1715 90. Jones P, Binns D, Chang HY, Fraser M, Li W, McAnulla C, et al.
1716 InterProScan 5: genome-scale protein function classification. Bioinformatics.
1717 2014;30(9):1236-40. Epub 2014/01/24. doi: 10.1093/bioinformatics/btu031.
1718 PubMed PMID: 24451626; PubMed Central PMCID: PMC3998142.
1719 91. Letunic I, Doerks T, Bork P. SMART: recent updates, new
1720 developments and status in 2015. Nucleic Acids Res. 2015;43(Database
1721 issue):D257-60. Epub 2014/10/11. doi: 10.1093/nar/gku949. PubMed PMID:
1722 25300481; PubMed Central PMCID: PMC4384020.
1723 92. Jorda J, Kajava AV. T-REKS: identification of Tandem REpeats in
1724 sequences with a K-meanS based algorithm. Bioinformatics.

2009;25(20):2632-8. Epub 2009/08/13. doi: 10.1093/bioinformatics/btp482. PubMed PMID: 19671691.

93. Zimmermann L, Stephens A, Nam SZ, Rau D, Kubler J, Lozajic M, et al. A completely reimplemented MPI bioinformatics toolkit with a new HHpred server at its core. J Mol Biol. 2018;430(15):2237-43. Epub 2017/12/21. doi: 10.1016/j.jmb.2017.12.007. PubMed PMID: 29258817.

94. Schardl CL, Young CA, Hesse U, Amyotte SG, Andreeva K, Calie PJ, et al. Plant-symbiotic fungi as chemical engineers: multi-genome analysis of the Clavicipitaceae reveals dynamics of alkaloid loci. PLoS Genetics. 2013;9(2):e1003323.

95. Kettles GJ, Bayon C, Canning G, Rudd JJ, Kanyuka K. Apoplastic recognition of multiple candidate effectors from the wheat pathogen *Zymoseptoria tritici* in the nonhost plant *Nicotiana benthamiana*. New Phytol. 2017;213(1):338-50. Epub 2016/10/04. doi: 10.1111/nph.14215. PubMed PMID: 27696417; PubMed Central PMCID: PMC5132004.

96. Bos JIB, Kanneganti T-D, Young C, Cakir C, Huitema E, Win J, et al. The C-terminal half of *Phytophthora infestans* RXLR effector AVR3a is sufficient to trigger R3a-mediated hypersensitivity and suppress INF1-induced cell death in *Nicotiana benthamiana*. Plant J. 2006;48(2):165-76. Epub 2006/09/13. doi: 10.1111/j.1365-313X.2006.02866.x. PubMed PMID: 16965554.

97. Ma LJ, van der Does HC, Borkovich KA, Coleman JJ, Daboussi MJ, Di Pietro A, et al. Comparative genomics reveals mobile pathogenicity chromosomes in *Fusarium*. Nature. 2010;464(7287):367-73. Epub 2010/03/20. doi: nature08850 [pii]

10.1038/nature08850. PubMed PMID: 20237561.

98. van Dam P, Fokkens L, Schmidt SM, Linmans JH, Kistler HC, Ma LJ, et al. Effector profiles distinguish formae speciales of *Fusarium oxysporum*. Environ Microbiol. 2016;18(11):4087-102. doi: 10.1111/1462-2920.13445. PubMed PMID: 27387256.

99. Inoue Y, Vy TTP, Yoshida K, Asano H, Mitsuoka C, Asuke S, et al. Evolution of the wheat blast fungus through functional losses in a host specificity determinant. Science. 2017;357(6346):80-3. Epub 2017/07/08. doi: 10.1126/science.aam9654. PubMed PMID: 28684523.

100. Yoshida K, Saitoh H, Fujisawa S, Kanzaki H, Matsumura H, Yoshida K, et al. Association genetics reveals three novel avirulence genes from the rice blast fungal pathogen *Magnaporthe oryzae*. Plant Cell. 2009;21(5):1573-91. Epub 2009/05/21. doi: 10.1105/tpc.109.066324. PubMed PMID: 19454732; PubMed Central PMCID: PMC2700537.

101. Ridout CJ, Skamnioti P, Porritt O, Sacristan S, Jones JD, Brown JK. Multiple avirulence paralogues in cereal powdery mildew fungi may contribute to parasite fitness and defeat of plant resistance. Plant Cell. 2006;18(9):2402-14. doi: 10.1105/tpc.106.043307. PubMed PMID: 16905653; PubMed Central PMCID: PMC1560912.

102. Houterman PM, Cornelissen BJ, Rep M. Suppression of plant resistance gene-based immunity by a fungal effector. PLoS Pathog. 2008;4(5):e1000061. Epub 2008/05/10. doi: 10.1371/journal.ppat.1000061. PubMed PMID: 18464895; PubMed Central PMCID: PMC2330162.

103. Selin C, de Kievit TR, Belmonte MF, Fernando WG. Elucidating the role of effectors in plant-fungal interactions: progress and challenges.

1775 Frontiers in microbiology. 2016;7:600. Epub 2016/05/21. doi:
1776 10.3389/fmicb.2016.00600. PubMed PMID: 27199930; PubMed Central
1777 PMCID: PMC4846801.
1778 104. Lu C, Chen J, Zhang Y, Hu Q, Su W, Kuang H. Miniature inverted-
1779 repeat transposable elements (MITEs) have been accumulated through
1780 amplification bursts and play important roles in gene expression and species
1781 diversity in *Oryza sativa*. Mol Biol Evol. 2012;29(3):1005-17. Epub
1782 2011/11/19. doi: 10.1093/molbev/msr282. PubMed PMID: 22096216; PubMed
1783 Central PMCID: PMC3278479.
1784 105. Fleetwood DJ, Scott B, Lane GA, Tanaka A, Johnson RD. A complex
1785 ergovaline gene cluster in epichloë endophytes of grasses. Appl Environ
1786 Microbiol. 2007;73(8):2571-9. PubMed PMID: 17308187.
1787 106. van Dam P, Fokkens L, Ayukawa Y, van der Gragt M, Ter Horst A,
1788 Brankovics B, et al. A mobile pathogenicity chromosome in *Fusarium*
1789 *oxysporum* for infection of multiple cucurbit species. Sci Rep. 2017;7(1):9042.
1790 Epub 2017/08/24. doi: 10.1038/s41598-017-07995-y. PubMed PMID:
1791 28831051; PubMed Central PMCID: PMC5567276.
1792 107. Bolton MD, van Esse HP, Vossen JH, de Jonge R, Stergiopoulos I,
1793 Stulemeijer IJE, et al. The novel *Cladosporium fulvum* lysin motif effector
1794 Ecp6 is a virulence factor with orthologues in other fungal species. Mol
1795 Microbiol. 2008;69(1):119-36. Epub 2008/05/03. doi: 10.1111/j.1365-
1796 2958.2008.06270.x. PubMed PMID: 18452583.
1797 108. Vargas WA, Sanz-Martín JM, Rech GE, Armijos-Jaramillo VD, Rivera
1798 LP, Echeverria MM, et al. A fungal effector with host nuclear localization and
1799 DNA-binding properties is required for maize anthracnose development. Mol

1800 Plant-Microbe Interact. 2016;29(2):83-95. Epub 2015/11/12. doi:
1801 10.1094/MPMI-09-15-0209-R. PubMed PMID: 26554735.
1802 109. Mesarich CH, Bowen JK, Hamiaux C, Templeton MD. Repeat-
1803 containing protein effectors of plant-associated organisms. Front Plant Sci.
1804 2015;6:872. Epub 2015/11/12. doi: 10.3389/fpls.2015.00872. PubMed PMID:
1805 26557126; PubMed Central PMCID: PMC4617103.
1806 110. Grove TZ, Cortajarena AL, Regan L. Ligand binding by repeat proteins:
1807 natural and designed. Curr Opin Struct Biol. 2008;18(4):507-15. Epub
1808 2008/07/08. doi: 10.1016/j.sbi.2008.05.008. PubMed PMID: 18602006;
1809 PubMed Central PMCID: PMCPMC3500881.
1810 111. Johnson RD, Lane GA, Koulman A, Cao M, Fraser K, Fleetwood DJ, et
1811 al. A novel family of cyclic oligopeptides derived from ribosomal peptide
1812 synthesis of an in planta-induced gene, *gigA*, in *Epichloë* endophytes of
1813 grasses. Fungal Genet Biol. 2015;85:14-24. doi: 10.1016/j.fgb.2015.10.005.
1814 PubMed PMID: 26519220.
1815 112. Wosten HA, Bohlmann R, Eckerskorn C, Lottspeich F, Bolker M,
1816 Kahmann R. A novel class of small amphipathic peptides affect aerial hyphal
1817 growth and surface hydrophobicity in *Ustilago maydis*. EMBO J.
1818 1996;15(16):4274-81. Epub 1996/08/15. PubMed PMID: 8861956; PubMed
1819 Central PMCID: PMC452153.
1820 113. Teertstra WR, van der Velden GJ, de Jong JF, Kruijtzer JA, Liskamp
1821 RM, Kroon-Batenburg LM, et al. The filament-specific Rep1-1 repellent of the
1822 phytopathogen *Ustilago maydis* forms functional surface-active amyloid-like
1823 fibrils. J Biol Chem. 2009;284(14):9153-9. Epub 2009/01/24. doi:

1824 10.1074/jbc.M900095200. PubMed PMID: 19164282; PubMed Central
1825 PMCID: PMCPMC2666566.
1826 114. Christensen MJ, Bennett RJ, Ansari HA, Koga H, Johnson RD, Bryan
1827 GT, et al. *Epichloë* endophytes grow by intercalary hyphal extension in
1828 elongating grass leaves. Fungal Genet Biol. 2008;45:84-93.
1829 115. Voisey CR. Intercalary growth in hyphae of filamentous fungi. Fungal
1830 Biol Rev. 2010;24:123-31.
1831 116. Bultman TL, Leuchtmann A. Biology of the *Epichloë-Botanophila*
1832 interaction: an intriguing association between fungi and insects. Fungal Biol
1833 Rev. 2009;22:131-8.
1834 117. Stewart EL, McDonald BA. Measuring quantitative virulence in the
1835 wheat pathogen *Zymoseptoria tritici* using high-throughput automated image
1836 analysis. Phytopathology. 2014;104(9):985-92. Epub 2014/03/15. doi:
1837 10.1094/PHYTO-11-13-0328-R. PubMed PMID: 24624955.
1838 118. Stewart EL, Hagerty CH, Mikaberidze A, Mundt CC, Zhong Z,
1839 McDonald BA. An improved method for measuring quantitative resistance to
1840 the wheat pathogen *Zymoseptoria tritici* using high-throughput automated
1841 image analysis. Phytopathology. 2016;106(7):782-8. Epub 2016/04/07. doi:
1842 10.1094/PHYTO-01-16-0018-R. PubMed PMID: 27050574.
1843 119. Wessling R, Epple P, Altmann S, He Y, Yang L, Henz SR, et al.
1844 Convergent targeting of a common host protein-network by pathogen
1845 effectors from three kingdoms of life. Cell host & microbe. 2014;16(3):364-75.
1846 Epub 2014/09/12. doi: 10.1016/j.chom.2014.08.004. PubMed PMID:
1847 25211078; PubMed Central PMCID: PMC4191710.

120. Win J, Chaparro-Garcia A, Belhaj K, Saunders DG, Yoshida K, Dong S, et al. Effector biology of plant-associated organisms: concepts and perspectives. Cold Spring Harbor symposia on quantitative biology. 2012;77:235-47. Epub 2012/12/12. doi: 10.1101/sqb.2012.77.015933. PubMed PMID: 23223409.

121. Heath MC. Nonhost resistance and nonspecific plant defenses. Curr Opin Plant Biol. 2000;3(4):315-9. PubMed PMID: 10873843.

122. Derevnina L, Dagdas YF, De la Concepcion JC, Bialas A, Kellner R, Petre B, et al. Nine things to know about elicitins. New Phytol. 2016;212(4):888-95. Epub 2016/09/02. doi: 10.1111/nph.14137. PubMed PMID: 27582271.

123. Du J, Verzaux E, Chaparro-Garcia A, Bijsterbosch G, Keizer LC, Zhou J, et al. Elicitin recognition confers enhanced resistance to *Phytophthora infestans* in potato. Nature plants. 2015;1(4):15034. Epub 2015/01/01. doi: 10.1038/nplants.2015.34. PubMed PMID: 27247034.

124. Dupont PY, Eaton CJ, Wargent JJ, Fechtner S, Solomon P, Schmid J, et al. Fungal endophyte infection of ryegrass reprograms host metabolism and alters development. New Phytol. 2015;208(4):1227-40. doi: 10.1111/nph.13614. PubMed PMID: 26305687.

125. Becker M, Becker Y, Green K, Scott B. The endophytic symbiont *Epichloë festucae* establishes an epiphyllous net on the surface of *Lolium perenne* leaves by development of an expressorium, an appressorium-like leaf exit structure. New Phytol. 2016;211:240-54. doi: 10.1111/nph.13931. PubMed PMID: 26991322.

1873

Supporting information

S1 File. Methods for computational analysis.

S1 Fig. Amino acid sequence alignments of E. festucae GpiB, SspM, SspN and SspO. Alignments of GpiB (A), SspM (B), SspN (C) and SspO (D) with homologs from a selection of *Epichloë* species. Red shading: Protease cleavage site; Green shading: omega site; Purple shading: *N*-glycosylation site; Orange shading: cysteine residues. Protein sequences for *E. baconii, E. elymi* and *E. typhina* were obtained from the Kentucky Endophyte database when available or predicted using FGENESH using *Claviceps purpurea* parameters. The deduced amino acid sequence was used for the alignment. Sequences marked with * were manually annotated.

S2 Fig. Strategy for deletion of the *E. festucae gpiB, sspM, sspN* and *sspO* genes and confirmation by Southern analysis. (A) Physical map of the *gpiB* WT genomic locus, linear insert of the *gpiB* replacement construct, pBH1, and the recombinant locus showing restriction enzyme sites for *Nde*I. Grey shading indicates regions of recombination. Numbers indicate the PCR primer pairs used for Gibson assembly (BH1/BH5) and deletion mutant screening (BH43/BH44). (B) PCR screening of deletion candidates with the PCR primer pair BH43/BH44, generated expected bands of 3,997 bp in WT, and 4,602 bp in deletion mutants (C) NBT/BCIP-stained Southern blot of digests (approx. 1 µg) from *E. festucae* WT, Δ*gpiB* T27, Δ*gpiB* T111 (PN3113), Δ*gpiB* T133 (PN3114), Δ*gpiB* T148 (PN3115), Δ*gpiB* T160 and Δ*gpiB* T204 strains probed

1899 with digoxigenin (DIG)-11-dUTP-labeled linear insert of pBH1 amplified with the
1900 primer pair BH1/BH5. Expected bands of 5,317 bp in WT, and 3,971 bp and
1901 1,951 bp in the deletion mutant.
1902 (D) Physical map of the *sspM* WT genomic locus, linear insert of the *sspM*
1903 replacement construct, pBH2, and the recombinant locus showing restriction
1904 enzyme sites for *EcoR*I. Grey shading indicates regions of recombination.
1905 Numbers indicate the PCR primer pairs used for Gibson assembly (BH9/BH12)
1906 and deletion mutant screening (BH45/BH46). (E) PCR screening of deletion
1907 candidates with the PCR primer pair BH45/BH46, generated expected bands
1908 of 3,615 bp in WT, and 4,190 bp in deletion mutants. (F) NBT/BCIP-stained
1909 Southern blot of digests (approx. 1 µg) of *E. festucae* WT, Δ*sspM* T180, Δ*sspM*
1910 T173, Δ*sspM* T163 (PN3118), Δ*sspM* T135, Δ*sspM* T99 (PN3117) and Δ*sspM*
1911 T52 (PN3116) strains probed with digoxigenin (DIG)-11-dUTP-labeled linear
1912 insert of pBH2 amplified with the primer pair BH9/BH12. Expected bands of
1913 2,205 bp and 1,569 bp in WT and 4,349 bp in the deletion mutant.
1914 (G) Physical map of the *sspN* WT genomic locus, linear insert of the *sspN*
1915 replacement construct, pBH3, and the recombinant locus showing restriction
1916 enzyme sites for *Bam*HI. Grey shading indicates regions of recombination.
1917 Numbers indicate the PCR primer pairs used for Gibson assembly
1918 (BH13/BH16) and deletion mutant screening (BH47/BH48). (H and J) PCR
1919 screening of deletion candidates with the PCR primer pair BH47/BH48,
1920 generated expected band of 3,403 bp in WT, and 4,250 bp in deletion mutants.
1921 (I) NBT/BCIP-stained Southern blot of digests (approx. 1 µg) of *E. festucae* WT,
1922 Δ*sspN* T151 and Δ*sspN* T10 (PN3119), strains probed with digoxigenin (DIG)-
1923 11-dUTP-labeled linear insert of pBH1 amplified with the primer pair

BH13/BH16. (K) NBT/BCIP-stained Southern blot of digests (approx. 1 µg) of *E. festucae* WT, Δ*sspN* T52 (PN3121), Δ*sspN* T15, Δ*sspN* T103, Δ*sspN* T51, Δ*sspN* T30 (PN3120) and Δ*sspN* T3 strains probed with digoxigenin (DIG)-11-dUTP-labeled linear insert of pBH3 amplified with the primer pair BH13/BH16. Expected bands of 1,710 bp and 3,631 bp in WT, and 1,710 bp and 4,477, in the deletion mutant.

(L) Physical map of the *sspO* WT genomic locus, linear insert of the *sspO* replacement construct, pBH4, and the recombinant locus showing restriction enzyme sites for *Pst*I. Grey shading indicates regions of recombination. Numbers indicate the PCR primer pairs used for Gibson assembly (BH5/BH9) and deletion mutant screening (BH49/BH50). (M) PCR screening of deletion candidates with the PCR primer pair BH49/BH50, generated expected band of 3,654 bp in WT, and 4,482 bp in deletion mutants. (N) NBT/BCIP-stained Southern blot of digests (approx. 1 µg) of *E. festucae* WT, Δ*sspO* T210 (PN3124), Δ*sspO* T195 (PN3123), ΔsspO T130, Δ*sspO* T102, Δ*sspO* T78 (PN3122) and Δ*sspO* T60 strains probed with digoxigenin (DIG)-11-dUTP-labeled linear insert of pBH4 amplified with the primer pair BH5/BH9. Expected bands of 1,859 bp and 1,678 bp in WT and 4,635 bp in the deletion mutant.

S3 Fig. Confocal laser scanning microscopy of aniline blue and WGA-AF488 stained ovaries. The fungal endophytic cell wall was stained with aniline blue (orange pseudo colour) while fungal septa were stained with WGA-AF 488 (blue pseudo colour). A. Ovary of mutant strain Δ*sspM* T52, B. Ovary of mutant strain Δ*sspM* T163. *E. festucae* hyphae are marked by asterisk. Scale bar: 50 µm.

S4 Fig. qPCR and RT-qPCR results of the *gpiB, sspM, sspN* and *sspO* OE strains. (A) Copy number determined by qPCR is expressed relative to the WT copy number. Genes encoding *hepA* (single copy, light grey) and *pacC* (single copy, dark grey) were used as reference genes. (B) Expression level determined by RT-qPCR is expressed relative to the WT gene expression. The 40S ribosomal S22 gene was used as reference gene. Primers used for the analyses are given in S2 Table.

S5 Fig. Verification of the heterologous production of GpiB, SspM, SspN and SspO in *N. benthamiana* via western blotting. Total protein of the infiltrated leaf region was extracted and separated by electrophoresis on a 10% SDS gel. The gel was transferred to a membrane and probed with an anti-FLAG antibody. eGFP expressed in *N. benthamiana* served as positive control. Expected sizes: approx. 9.8 kDa for GpiB, 14 kDa for SspN, 10 kDa for SspO and for SspM 14.8 and 18.8 kDa.

S1 Table. Biosample references

S2 Table. Biological material.

S3 Table. Primers used in this study.

S4 Table. Summary of the presented information about *E. festucae* effector candidates.

S5 Table. Distribution of *gpiB* and the *ssps* within *Epichloë* and related species.

S6 Table. Vertical transmission of ssp mutants in *L. perenne*.

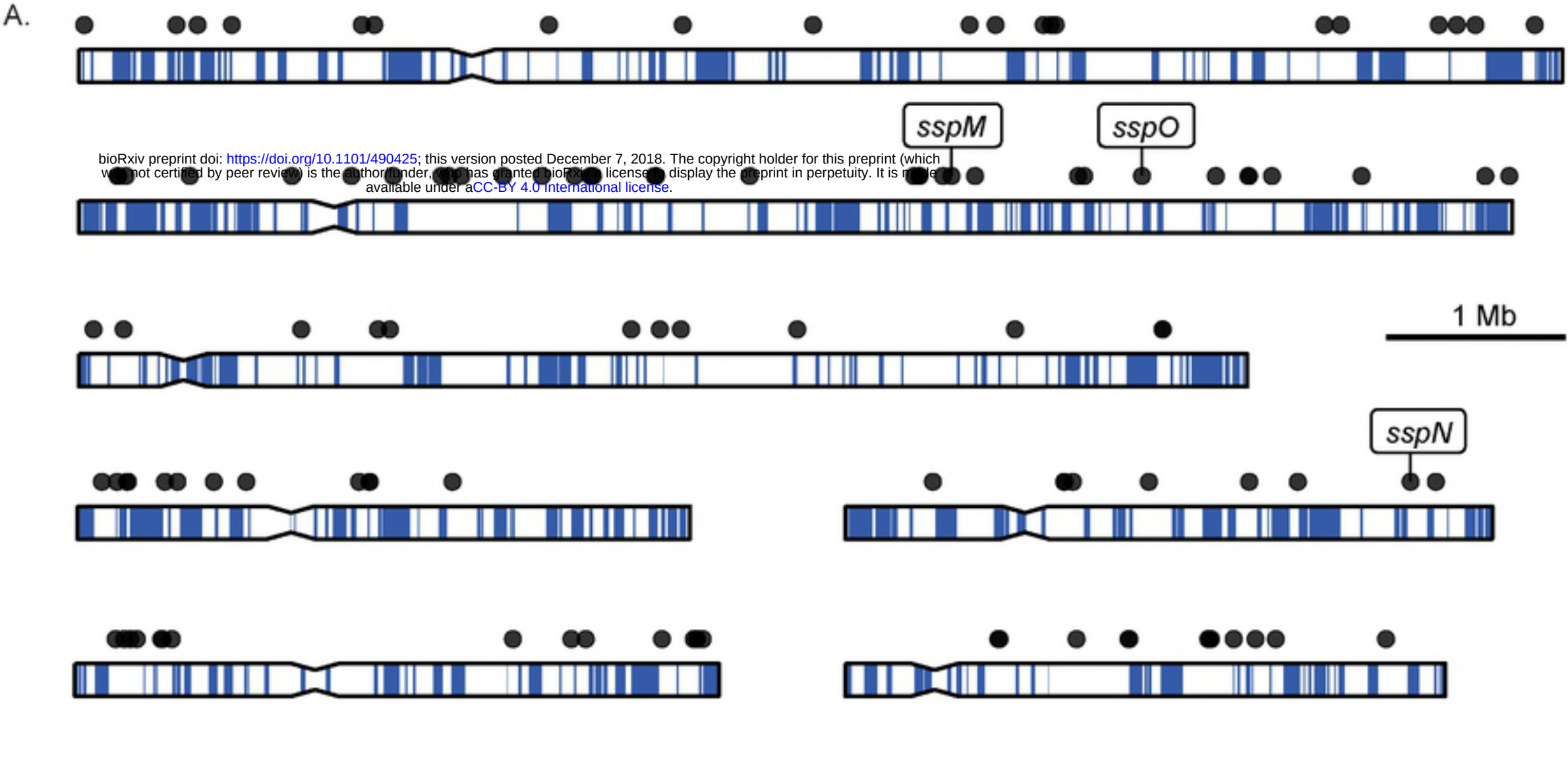

Figure 1

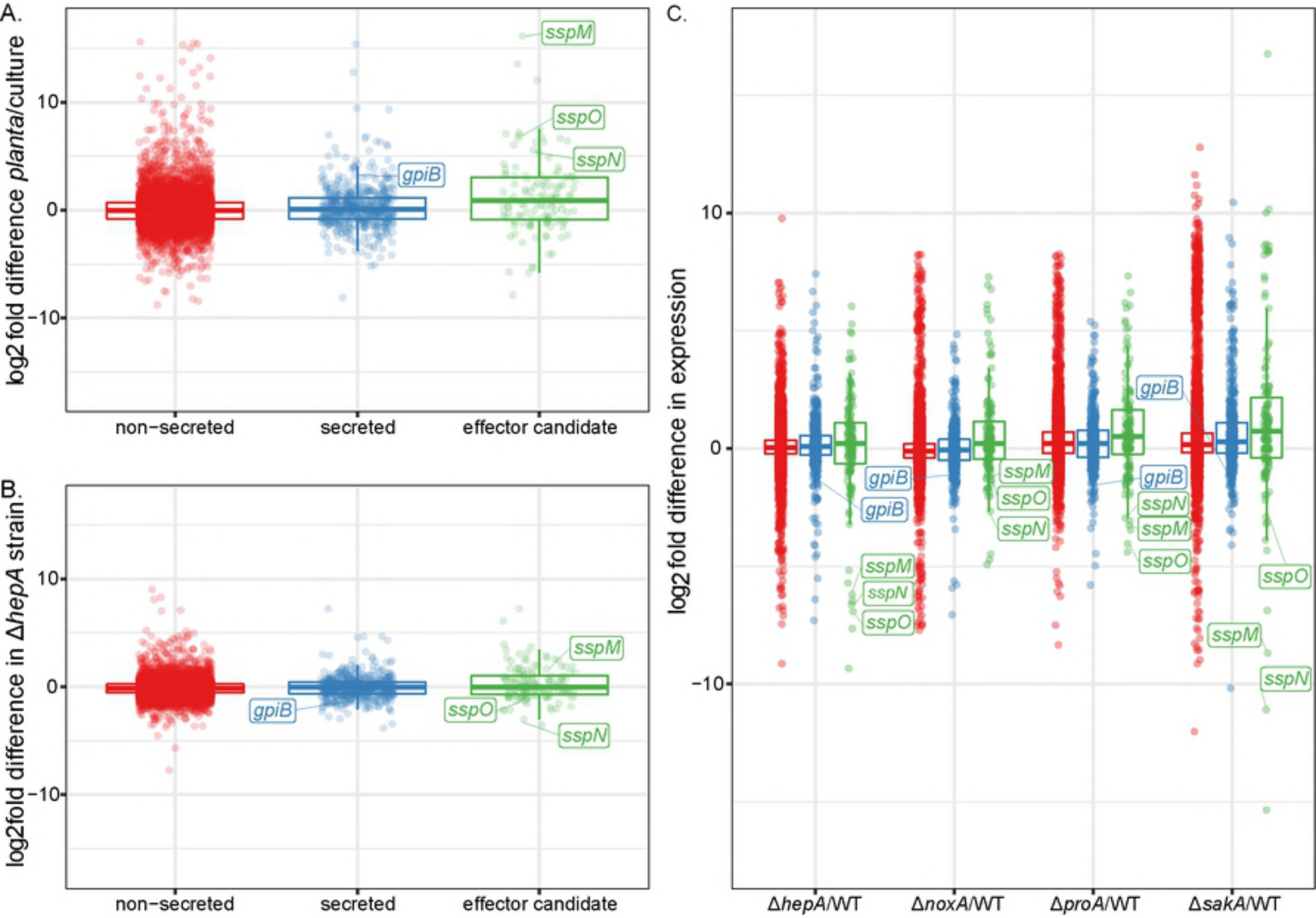
A.
log2 fold difference planta/culture
10
0
−10
sspM
sspO
sspN
gpiB
non−secreted
secreted
effector candidate
B.
log2fold difference in ΔhepA strain
10
0
−10
gpiB
sspO
sspM
sspN
non−secreted
secreted
effector candidate
C.
log2 fold difference in expression
10
0
−10
gpiB
gpiB
gpiB
sspM
sspO
sspN
sspM
sspN
sspO
gpiB
sspN
sspM
sspO
sspO
sspM
sspN
ΔhepA/WT
ΔnoxA/WT
ΔproA/WT
ΔsakA/WT

Figure 2

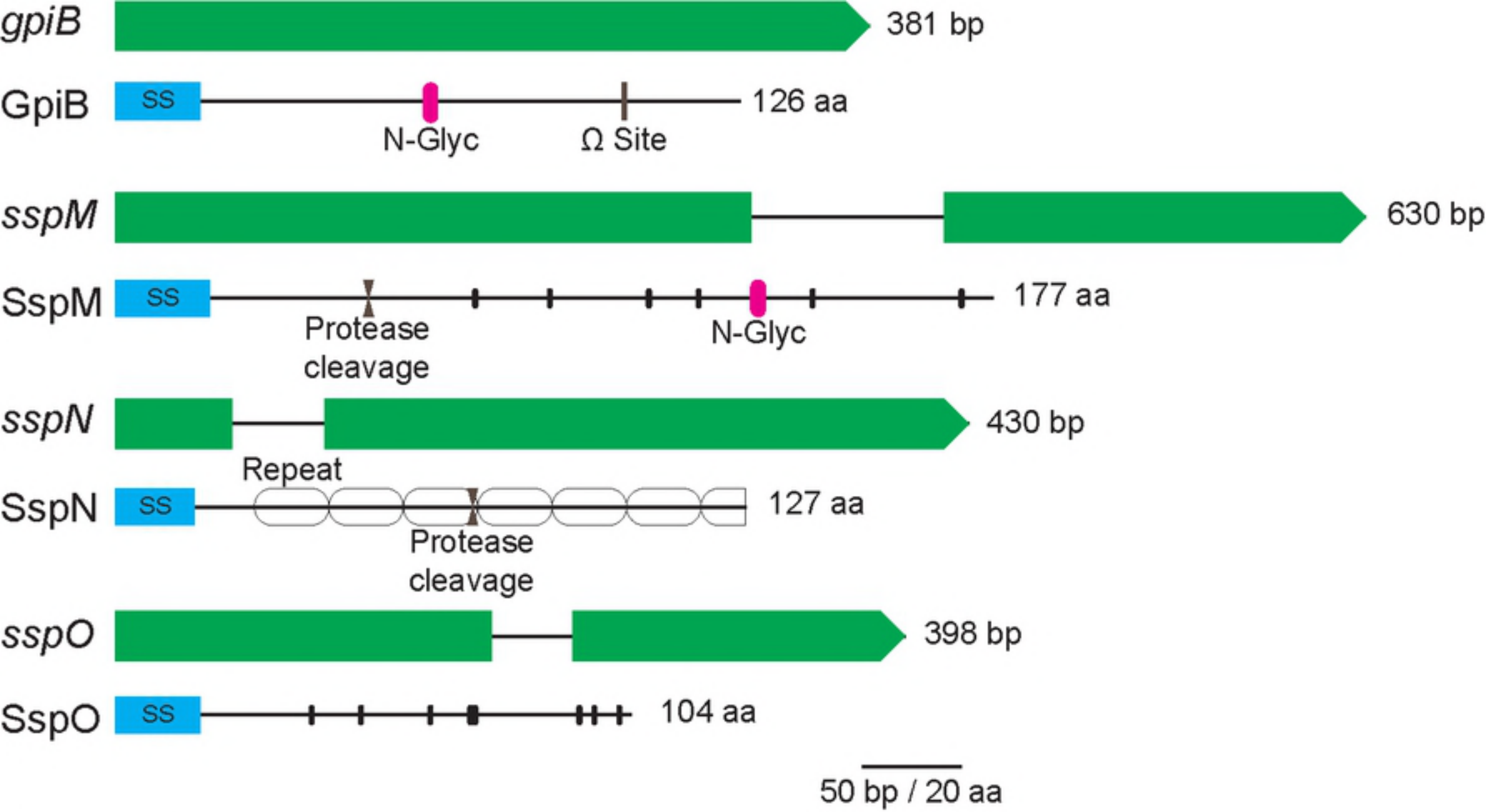
gpiB
381 bp
GpiB
SS
126 aa
N-Glyc
Ω Site
sspM
630 bp
SspM
SS
177 aa
Protease
cleavage
N-Glyc
sspN
430 bp
Repeat
SspN
SS
127 aa
Protease
cleavage
sspO
398 bp
SspO
SS
104 aa
50 bp / 20 aa

Figure 3

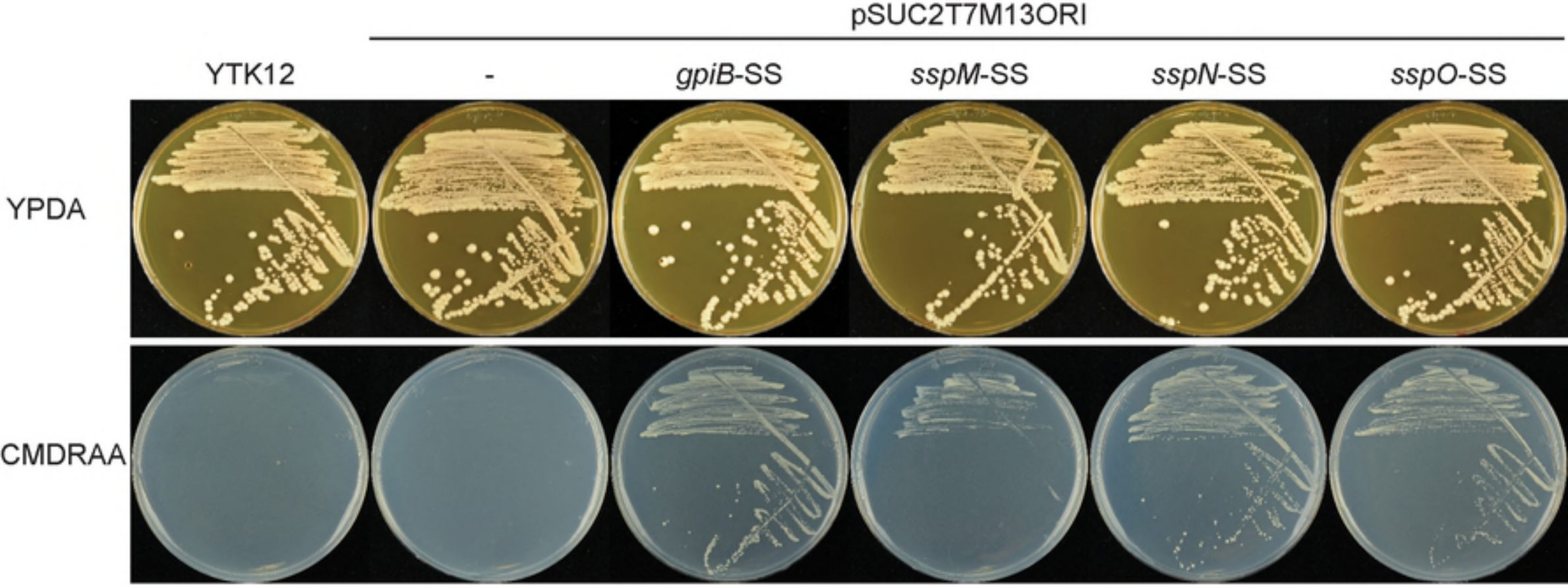
pSUC2T7M13ORI
YTK12
-
gpiB-SS
sspM-SS
sspN-SS
sspO-SS
YPDA
CMDRAA

Figure 4

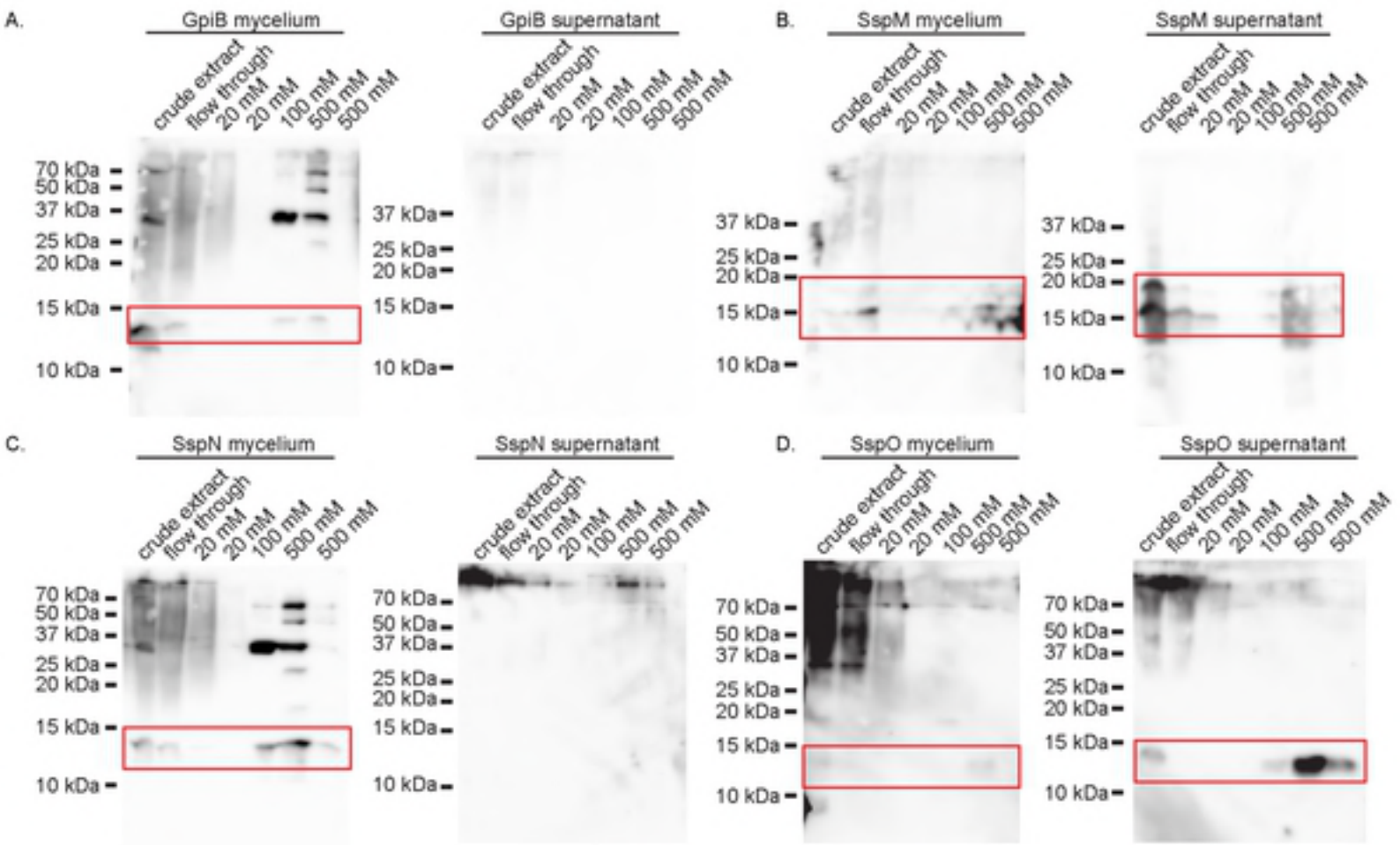
A.
GpiB mycelium
GpiB supernatant
crude extract
flow through
20 mM
20 mM
100 mM
500 mM
500 mM
70 kDa
50 kDa
37 kDa
25 kDa
20 kDa
15 kDa
10 kDa
B.
SspM mycelium
SspM supernatant
C.
SspN mycelium
SspN supernatant
D.
SspO mycelium
SspO supernatant

Figure 5

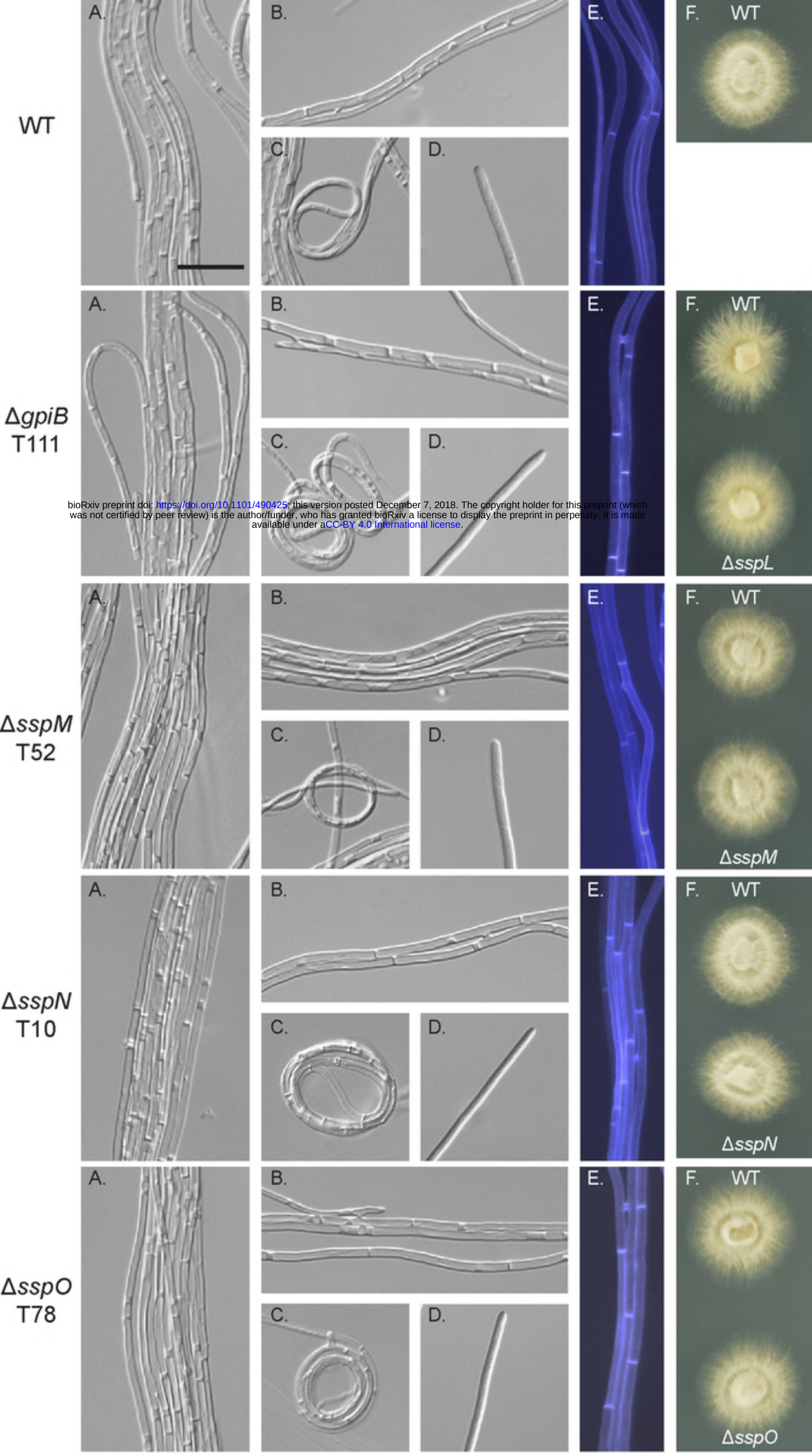

Figure 6

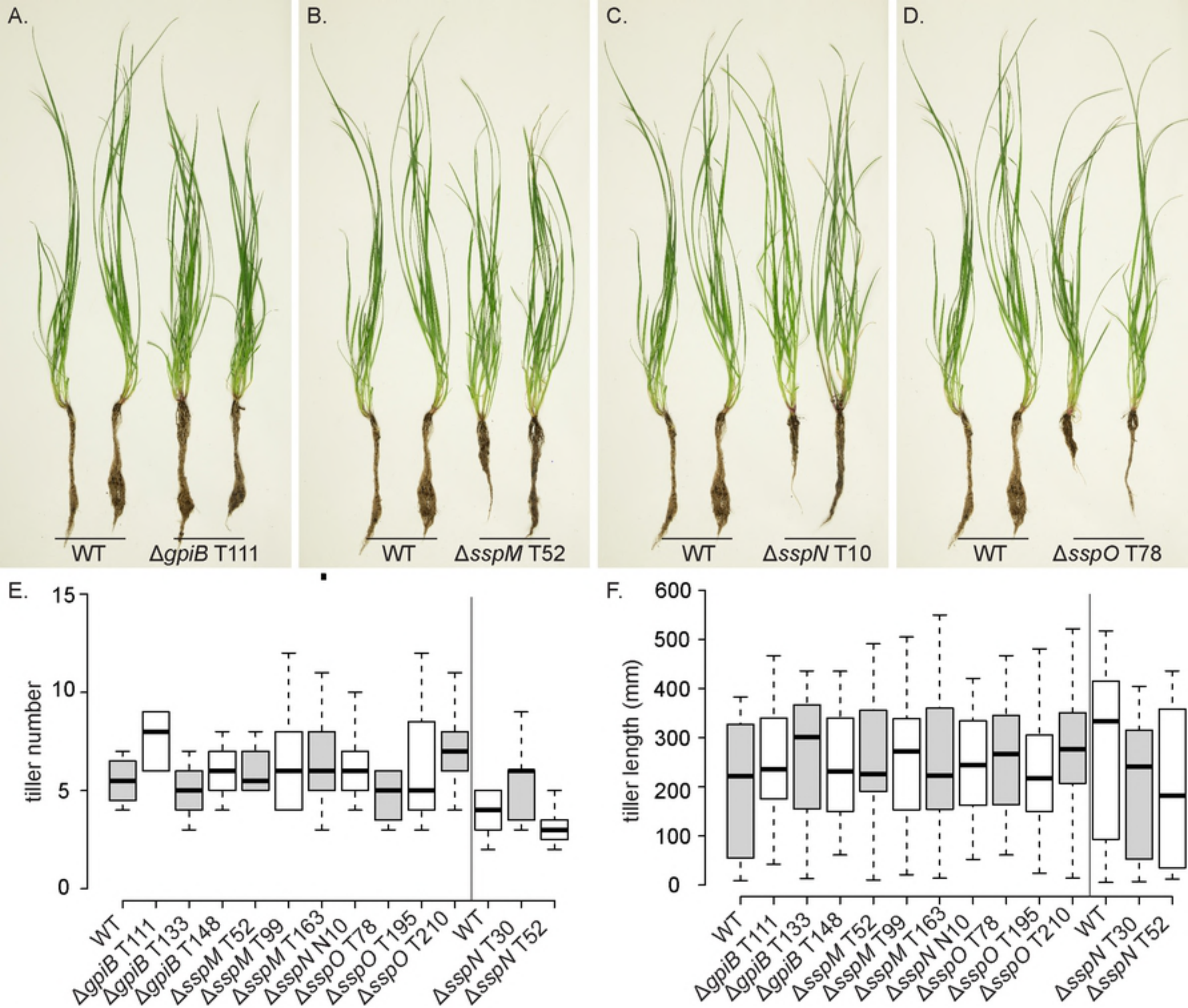
A.
WT
ΔgpiB T111
B.
WT
ΔsspM T52
C.
WT
ΔsspN T10
D.
WT
ΔsspO T78
E.
tiller number
0
5
10
15
WT
ΔgpiB T111
ΔgpiB T133
ΔgpiB T148
ΔsspM T52
ΔsspM T99
ΔsspM T163
ΔsspN N10
ΔsspO T78
ΔsspO T195
ΔsspO T210
WT
ΔsspN T30
ΔsspN T52
F.
tiller length (mm)
0
100
200
300
400
500
600
WT
ΔgpiB T111
ΔgpiB T133
ΔgpiB T148
ΔsspM T52
ΔsspM T99
ΔsspM T163
ΔsspN N10
ΔsspO T78
ΔsspO T195
ΔsspO T210
WT
ΔsspN T30
ΔsspN T52

Figure 7

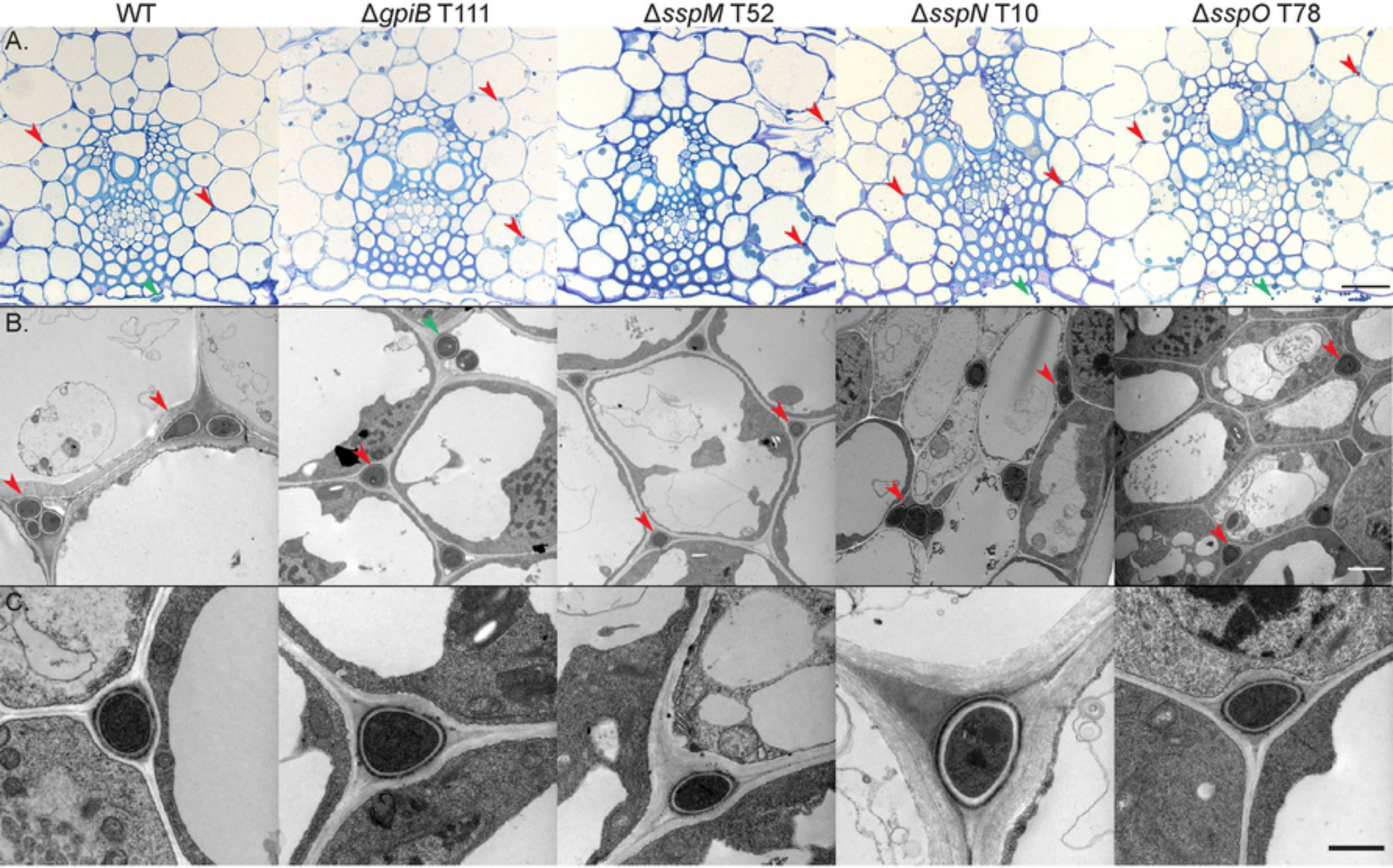

Figure 8

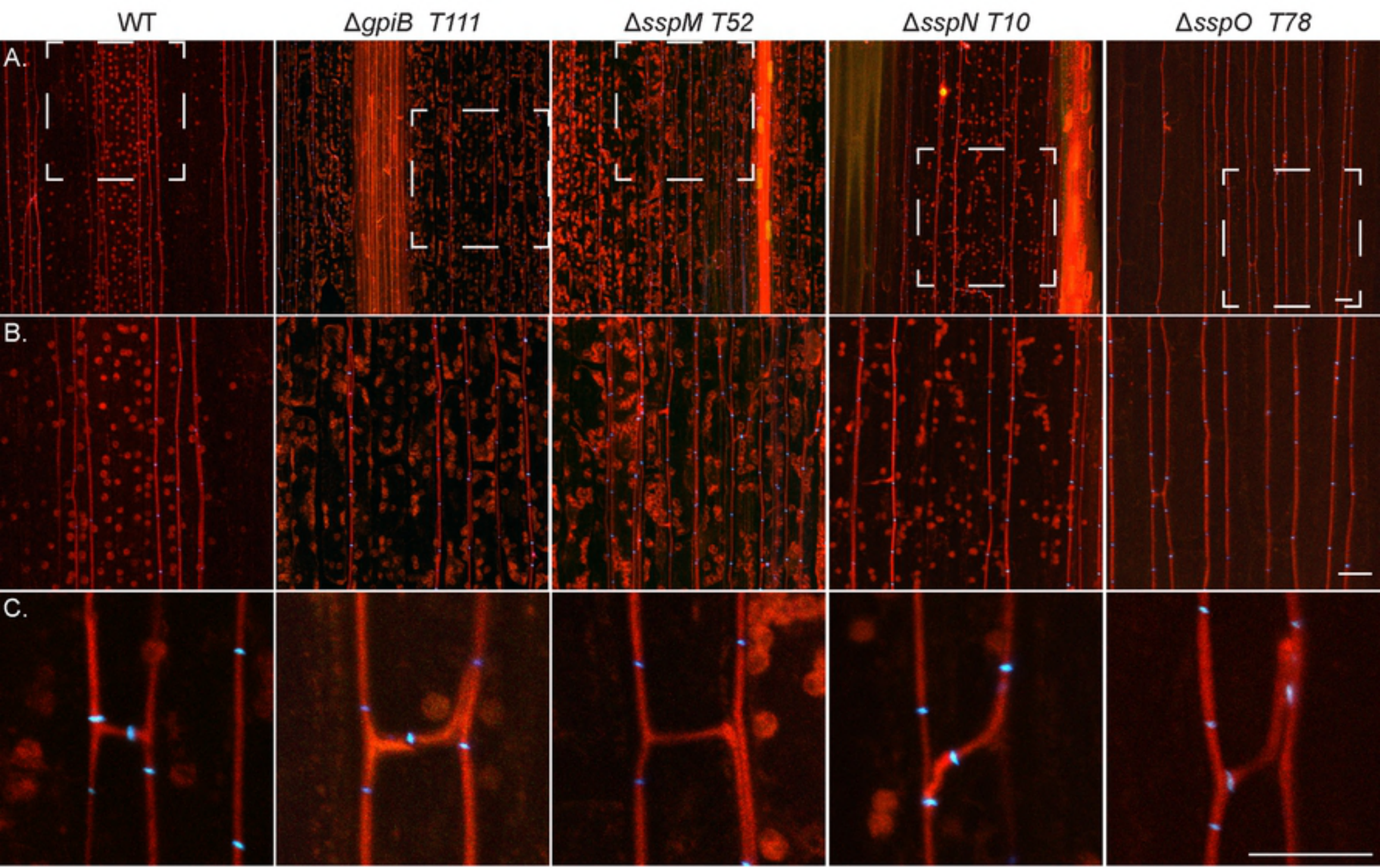

Figure 9

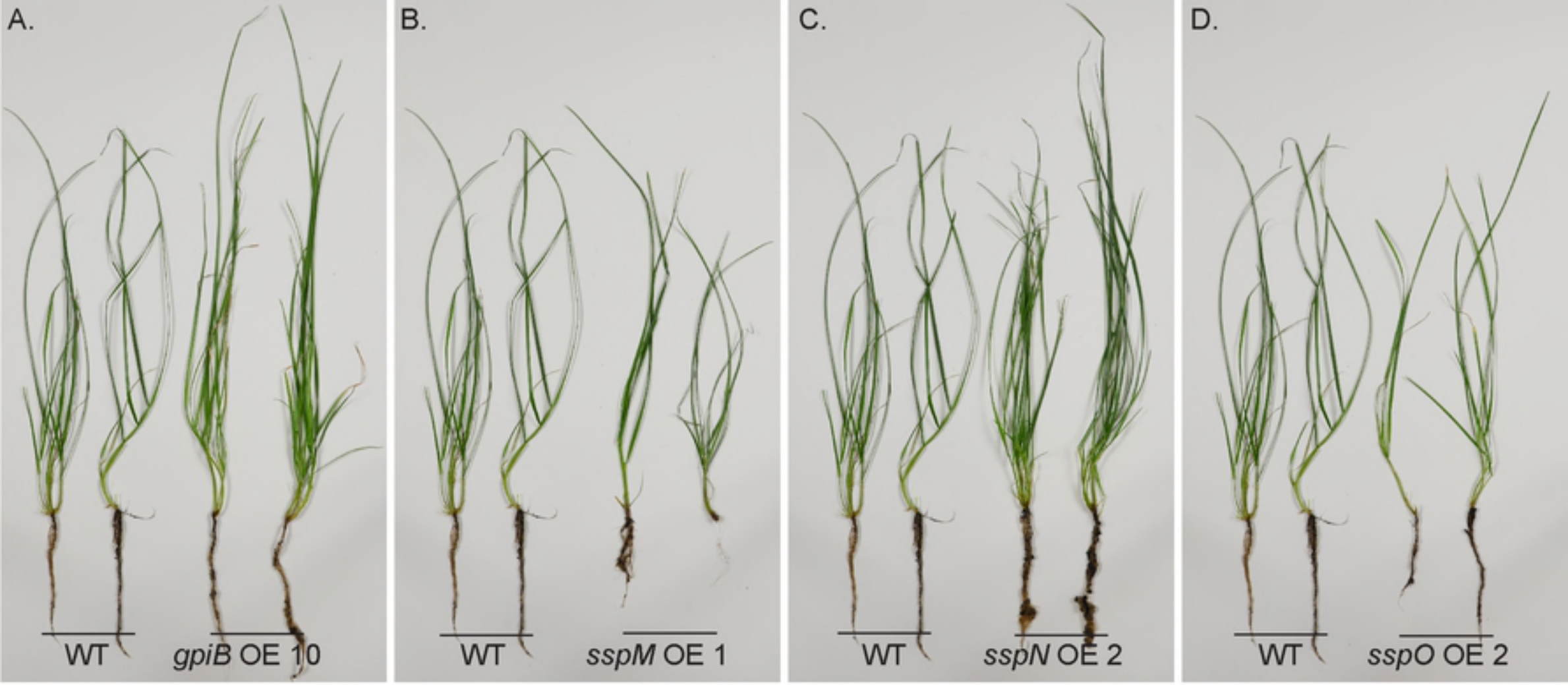
A.
WT
gpiB OE 10
B.
WT
sspM OE 1
C.
WT
sspN OE 2
D.
WT
sspO OE 2
E.
tiller number
0
2
4
6
8
10
WT
gpiB OE 2
gpiB OE 6
gpiB OE 10
sspM OE 1
sspM OE 6
sspM OE 10
sspN OE 2
sspN OE 4
sspN OE 7
sspO OE 2
sspO OE 3
F.
tiller length (mm)
0
100
200
300
400
500
600
WT
gpiB OE 2
gpiB OE 6
gpiB OE 10
sspM OE 1
sspM OE 6
sspM OE 10
sspN OE 2
sspN OE 4
sspN OE 7
sspO OE 2
sspO OE 3

Figure 10

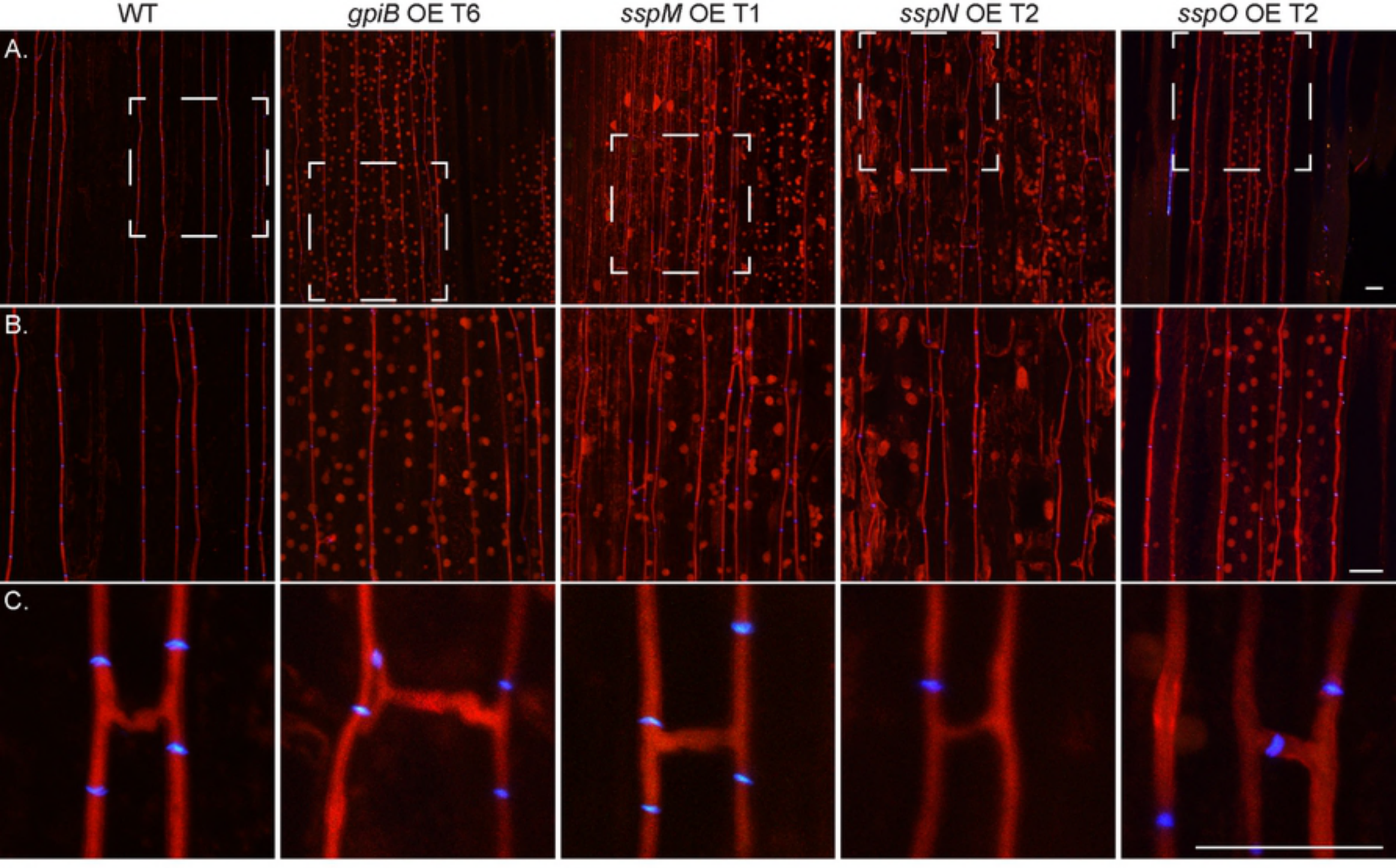

Figure 11

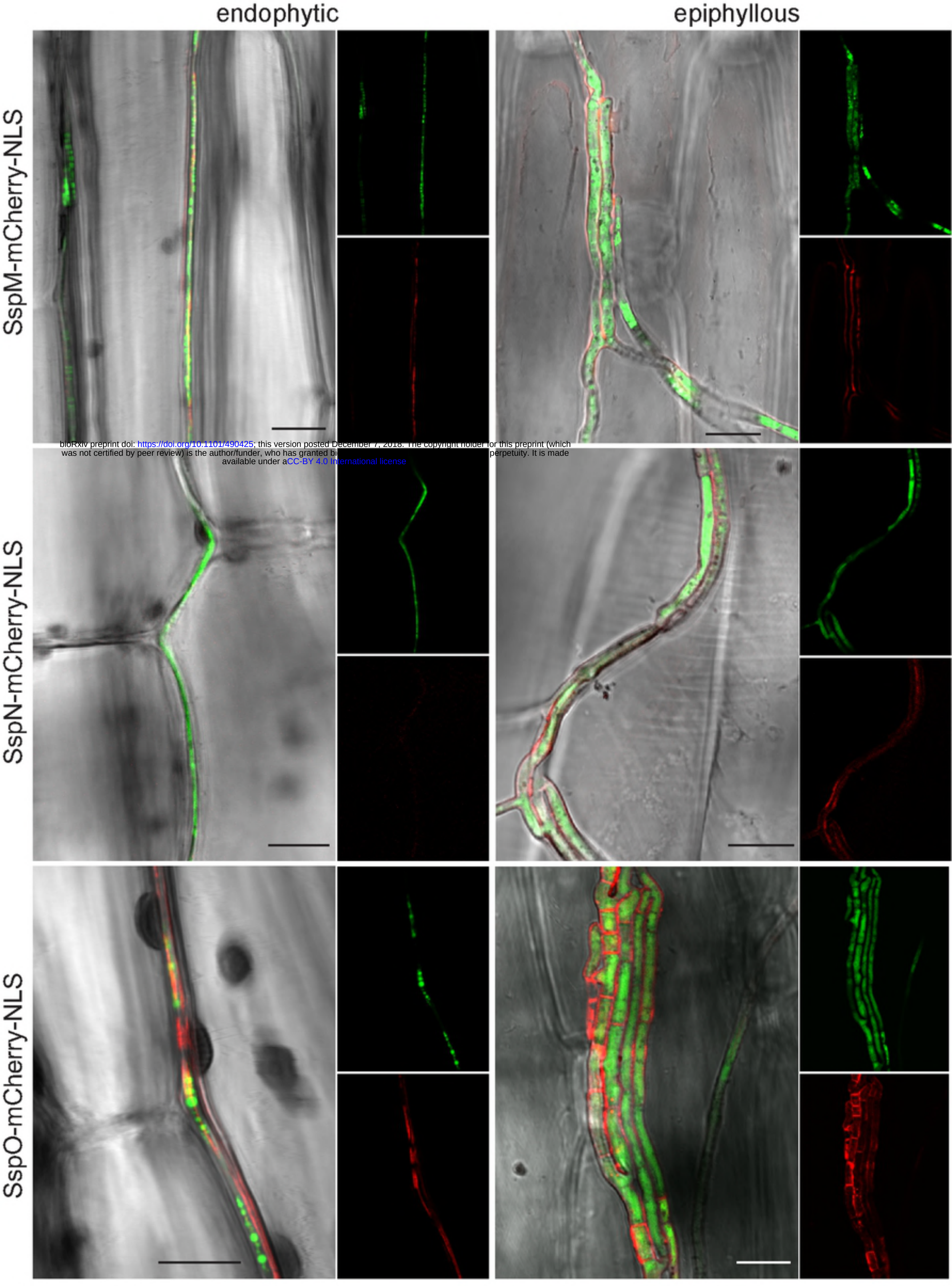

Figure 12

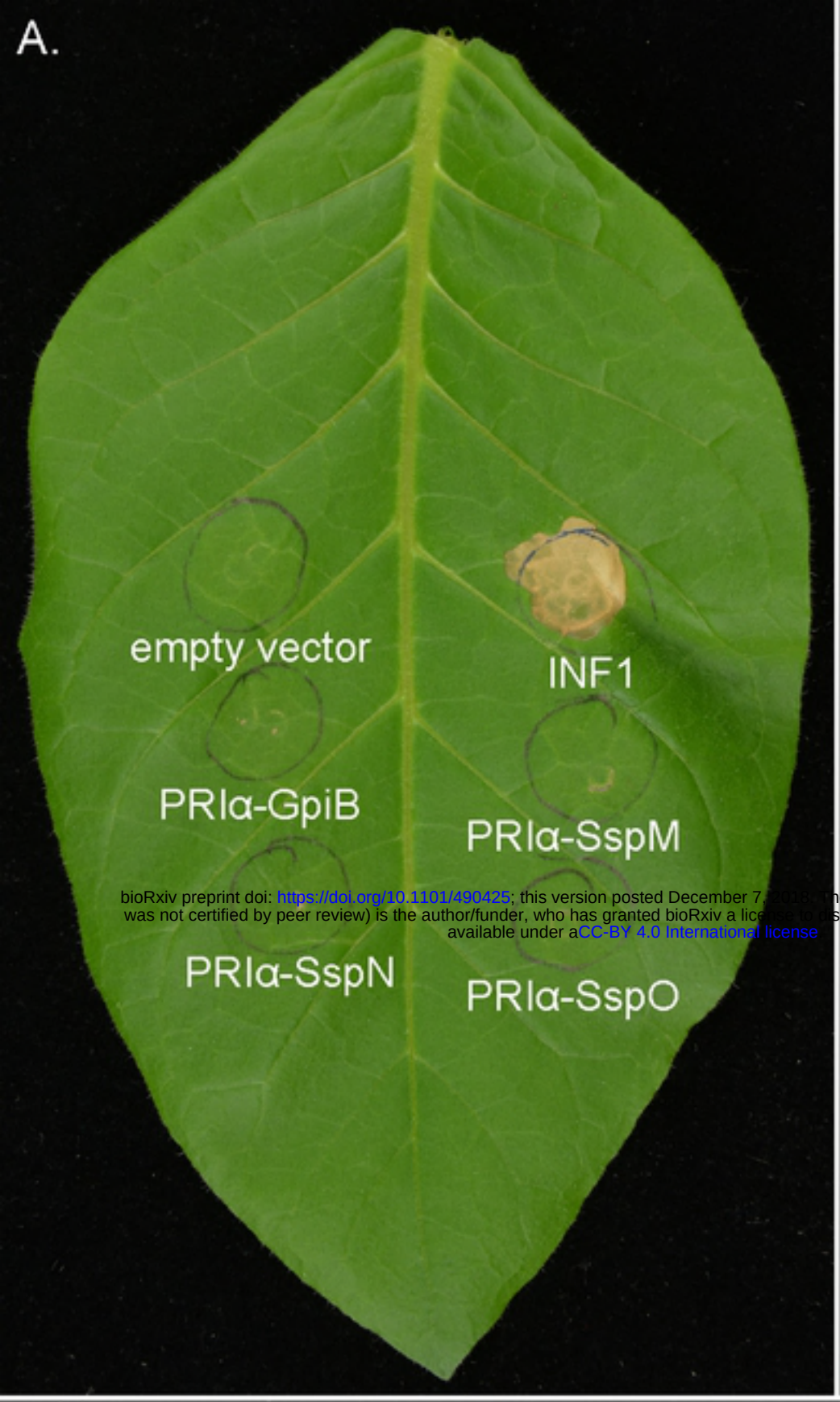

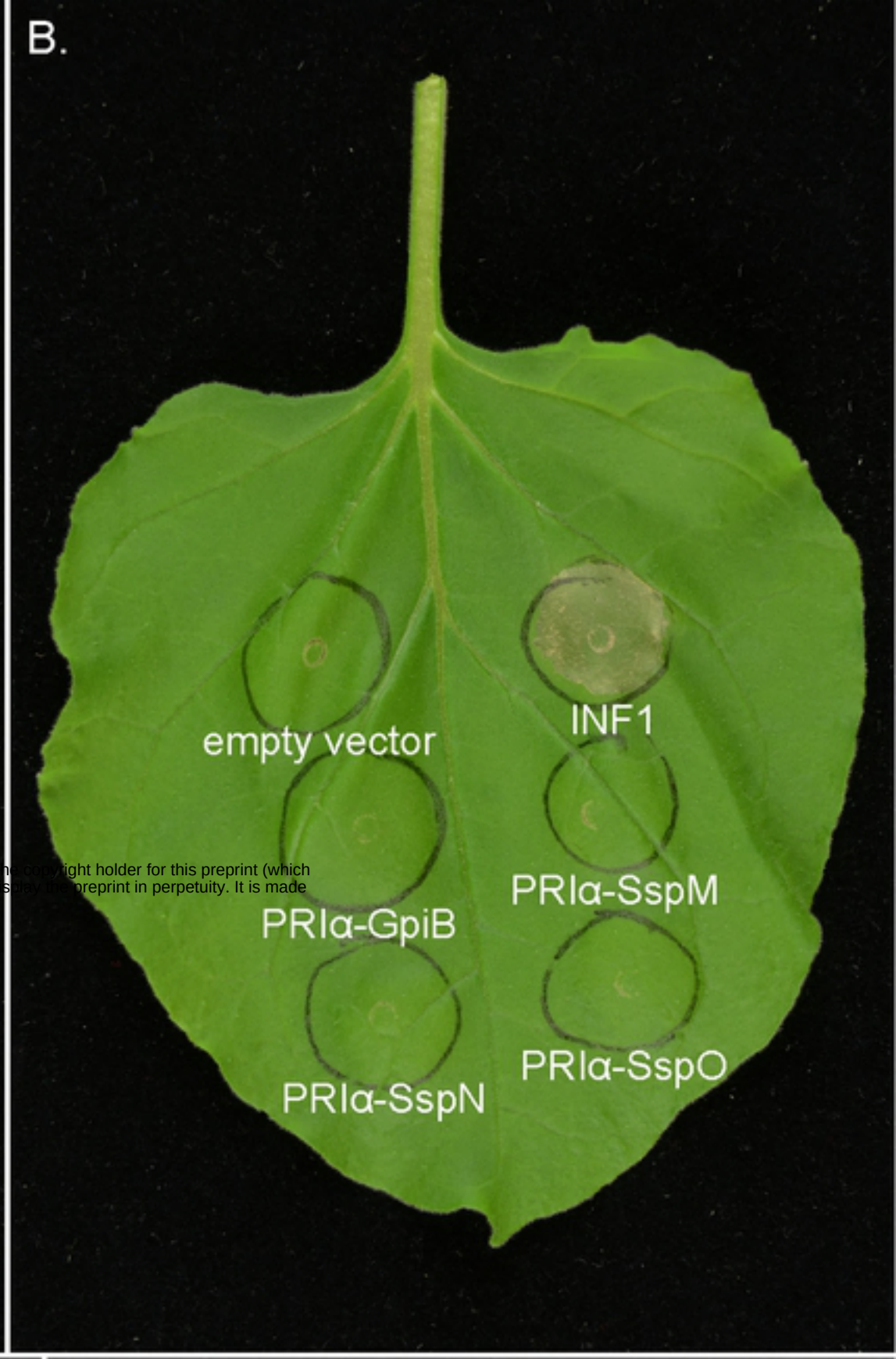

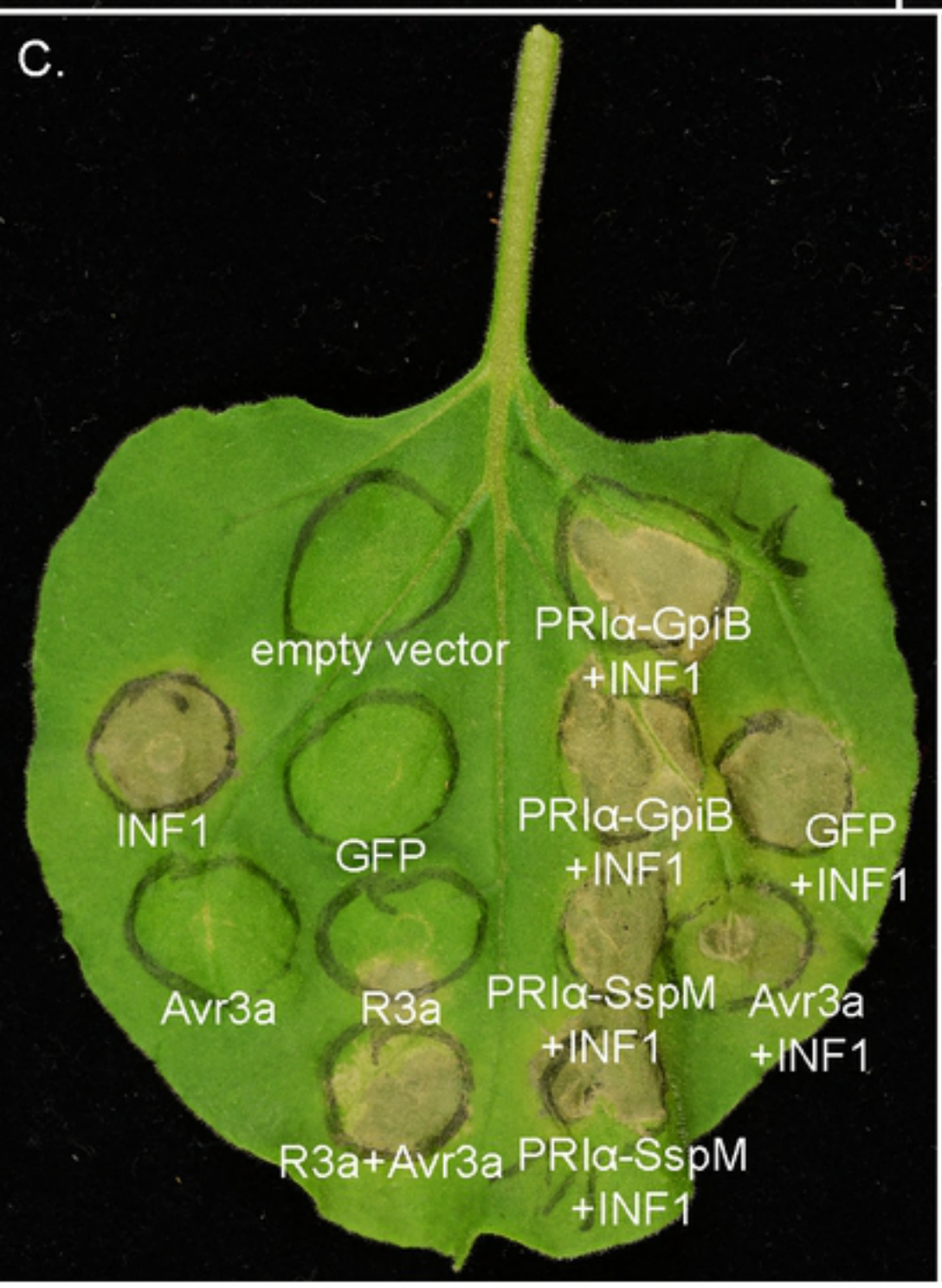

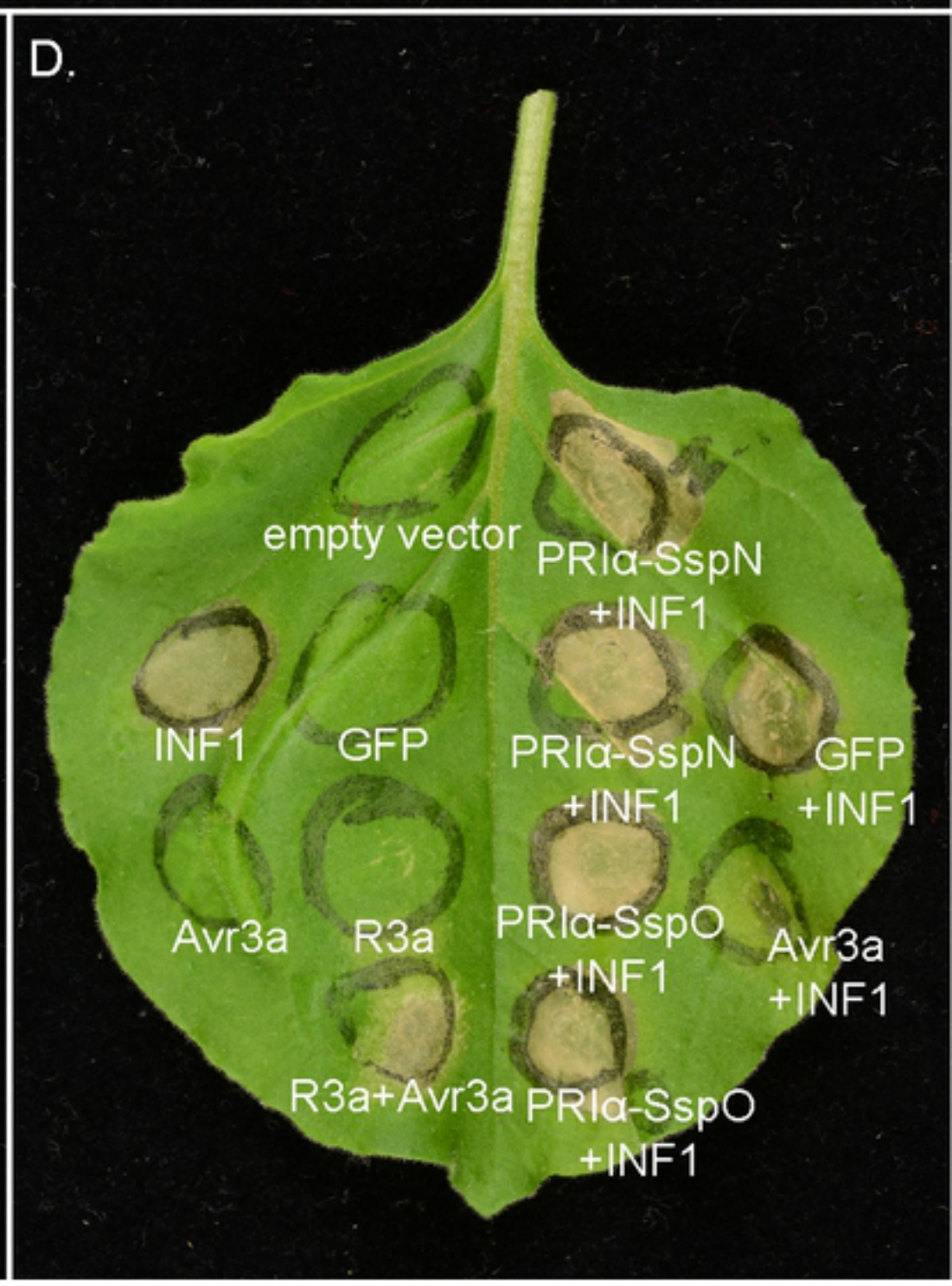

Figure 13